


Review

# Advances in Bi<sub>2</sub>WO<sub>6</sub>-Based Photocatalysts for Degradation of Organic Pollutants

Haiyan Jiang<sup>1</sup>, Jiahua He<sup>2</sup>, Changyi Deng<sup>2</sup>, Xiaodong Hong<sup>2,\*</sup>  and Bing Liang<sup>3</sup><sup>1</sup> Basic Department, Liaoning Institute of Science and Technology, Benxi 117004, China<sup>2</sup> School of Materials Science and Hydrogen Energy, Foshan University, Foshan 528000, China<sup>3</sup> College of Materials Science and Engineering, Shenyang University of Chemical Technology, Shenyang 110142, China

\* Correspondence: hongxiaodong@lntu.edu.cn

**Abstract:** With the rapid development of modern industries, water pollution has become an urgent problem that endangers the health of human and wild animals. The photocatalysis technique is considered an environmentally friendly strategy for removing organic pollutants in wastewater. As an important member of Bi-series semiconductors, Bi<sub>2</sub>WO<sub>6</sub> is widely used for fabricating high-performance photocatalysts. In this review, the recent advances of Bi<sub>2</sub>WO<sub>6</sub>-based photocatalysts are summarized. First, the controllable synthesis, surface modification and heteroatom doping of Bi<sub>2</sub>WO<sub>6</sub> are introduced. In the respect of Bi<sub>2</sub>WO<sub>6</sub>-based composites, existing Bi<sub>2</sub>WO<sub>6</sub>-containing binary composites are classified into six types, including Bi<sub>2</sub>WO<sub>6</sub>/carbon or MOF composite, Bi<sub>2</sub>WO<sub>6</sub>/g-C<sub>3</sub>N<sub>4</sub> composite, Bi<sub>2</sub>WO<sub>6</sub>/metal oxides composite, Bi<sub>2</sub>WO<sub>6</sub>/metal sulfides composite, Bi<sub>2</sub>WO<sub>6</sub>/Bi-series composite, and Bi<sub>2</sub>WO<sub>6</sub>/metal tungstates composite. Bi<sub>2</sub>WO<sub>6</sub>-based ternary composites are classified into four types, including Bi<sub>2</sub>WO<sub>6</sub>/g-C<sub>3</sub>N<sub>4</sub>/X, Bi<sub>2</sub>WO<sub>6</sub>/carbon/X, Bi<sub>2</sub>WO<sub>6</sub>/Au or Ag-based materials/X, and Bi<sub>2</sub>WO<sub>6</sub>/Bi-series semiconductors/X. The design, microstructure, and photocatalytic performance of Bi<sub>2</sub>WO<sub>6</sub>-based binary and ternary composites are highlighted. Finally, aimed at the existing problems in Bi<sub>2</sub>WO<sub>6</sub>-based photocatalysts, some solutions and promising research trends are proposed that would provide theoretical and practical guidelines for developing high-performance Bi<sub>2</sub>WO<sub>6</sub>-based photocatalysts.

**Keywords:** Bi<sub>2</sub>WO<sub>6</sub>; photocatalysis; degradation performance; composite



**Citation:** Jiang, H.; He, J.; Deng, C.; Hong, X.; Liang, B. Advances in Bi<sub>2</sub>WO<sub>6</sub>-Based Photocatalysts for Degradation of Organic Pollutants. *Molecules* **2022**, *27*, 8698. <https://doi.org/10.3390/molecules27248698>

Academic Editor: Ruowen Liang

Received: 20 November 2022

Accepted: 7 December 2022

Published: 8 December 2022

**Publisher's Note:** MDPI stays neutral with regard to jurisdictional claims in published maps and institutional affiliations.



**Copyright:** © 2022 by the authors. Licensee MDPI, Basel, Switzerland. This article is an open access article distributed under the terms and conditions of the Creative Commons Attribution (CC BY) license (<https://creativecommons.org/licenses/by/4.0/>).

## 1. Introduction

With the rapid development of various industries, pollution problems, including soil pollution, air pollution, and water pollution, are becoming more and more serious. The problem of water pollution is endangering the health of humans and wild animals; thus, wastewater treatment has become an important task of scientists and technicians. The photocatalysis technique is regarded as an environmentally friendly route for solving water pollution [1]. Therefore, the development of highly active photocatalysts is regarded as the major task of photocatalysis [2]. Lots of semiconductors are adopted as photocatalysts for the degradation of organic pollutants under the irradiation of visible light or UV light [3]. However, the general photocatalytic mechanism of different photocatalysts can be classified into the following three steps: The first step is the generation of photogenerated electrons and holes. When the light irradiation energy surpasses the energy gap (E<sub>g</sub>) of the semiconductor, the electrons jump from valence band (VB) to conduction band (CB) and leave holes in the VB [4]. The second step is the transfer of charge carriers. The electrons transfer to the surface of catalysts or recombine with holes. In this process, preventing the recombination of electrons and holes increases the lifetime of photogenerated electrons and holes and enhances the photocatalytic activity by prolonging the redox reaction time [5]. The last step is the surface redox reaction between electrons or holes with O<sub>2</sub> in H<sub>2</sub>O.

Consequently, highly active oxidants are produced and degrade organic pollutants into  $H_2O$  and  $CO_2$ , without secondary pollution. Based on the photocatalytic mechanism, the design principles of high-performance photocatalysts include, but are not limited to, enhancing the light harvesting capability and suppressing the recombination of electrons and holes [6].  $Bi_2WO_6$  is a commonly-used Bi-series semiconductor [7], which has widely served as a visible light photocatalyst for the degradation of organic pollutants due to its advantages of a perovskite-type layered structure, light harvesting ability (band gap of 2.8 eV), low cost, chemical stability, and non-toxicity [8]. In the respect of controllable synthesis, hydrothermal/solvothermal, sol-gel process, calcination, and electrodeposition can be used to prepare  $Bi_2WO_6$  nanoplates, nanosheets, nanorods, and nanoflowers or spheres. Besides microstructure control, surface modification and heteroatom doping are adopted for enhancing the photocatalytic activity through generating surface vacancies or defects. In addition, the construction of  $Bi_2WO_6$ -based composite photocatalysts has become the most popular research topic for the diversity of alternative semiconductive materials.

In view of the important role of  $Bi_2WO_6$  in Bi-series semiconductor photocatalysts, herein, we summarize the recent advances of  $Bi_2WO_6$ -based photocatalysts. Figure 1 shows that the whole review involves three sections. The first section is the controllable synthesis, surface modification, and heteroatom doping of  $Bi_2WO_6$ . In the second section, we majorly introduce the progress of  $Bi_2WO_6$ -based binary composite photocatalysts, including  $Bi_2WO_6$ /carbon or MOF composite,  $Bi_2WO_6$ /g- $C_3N_4$  composite,  $Bi_2WO_6$ /metal oxides composite,  $Bi_2WO_6$ /metal sulfides composite,  $Bi_2WO_6$ /Bi-series composite, and  $Bi_2WO_6$ /metal tungstates composite. In the last section,  $Bi_2WO_6$ -based ternary composites are reviewed, including  $Bi_2WO_6$ /g- $C_3N_4$ /X,  $Bi_2WO_6$ /carbon/X,  $Bi_2WO_6$ /Au or Ag-based materials/X, and  $Bi_2WO_6$ /Bi-series semiconductors/X. The design, microstructure, and photocatalytic performance of  $Bi_2WO_6$ -based binary and ternary composites are highlighted in detail. Lastly, we summarize the research highlights and existing problems in  $Bi_2WO_6$ -based photocatalysts. Based on the existing problems, some solutions and promising research trends are put forward, finally, that would provide theoretical and practical guidelines for developing novel  $Bi_2WO_6$ -based photocatalysts.

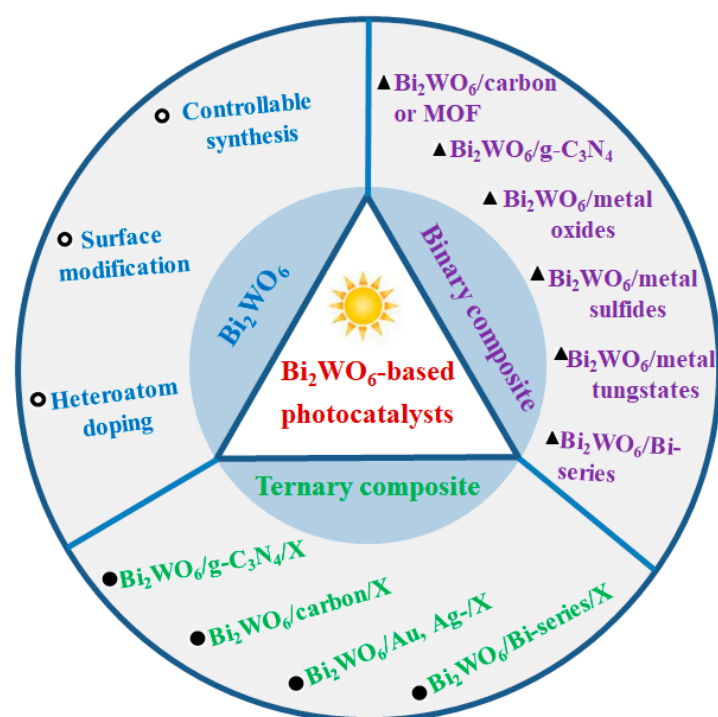


**Figure 1.** The related research directions of  $Bi_2WO_6$ -based photocatalysts.

## 2. Morphology Control, Surface Modification, and Heteroatom Doping of Bi<sub>2</sub>WO<sub>6</sub>

### 2.1. Morphology Control

The microstructure of Bi<sub>2</sub>WO<sub>6</sub> seriously affects the specific surface area and photocatalytic performance. Therefore, the controllable synthesis and surface modification of Bi<sub>2</sub>WO<sub>6</sub> have become the basic topic in preparing high-performance Bi<sub>2</sub>WO<sub>6</sub>-based photocatalysts. The synthetic methods of Bi<sub>2</sub>WO<sub>6</sub> include the hydrothermal/solvothermal method, sol-gel process and calcination, and the electrodeposition method. However, the hydrothermal and solvothermal methods have been widely adopted for fabricating Bi<sub>2</sub>WO<sub>6</sub>, due to the easy operation and controllable microstructure. In this respect, Lai et al. [9] synthesized various Bi<sub>2</sub>WO<sub>6</sub> photocatalysts via the solvothermal route and discussed the influence of reaction temperature on photocatalytic activity. The BWO-140 sample prepared at 140 °C delivered the best activity for the removal of Erichrome Black T (EBT) dye due to the oxygen vacancies, small size, and large surface area. Selvi et al. [10] discussed the influence of reaction time on the performance of Bi<sub>2</sub>WO<sub>6</sub> photocatalysts. Under the same hydrothermal conditions, the nanoplates of Bi<sub>2</sub>WO<sub>6</sub>-24 h delivered the optimum photocatalytic activity for the degradation of MB due to the narrow band, smaller crystallite size, and hierarchical structure.

### 2.2. Surface Modification

Besides the effect of reaction conditions, hexadecyl trimethyl ammonium bromide (CTAB) and polyvinylpyrrolidone (PVP) are adopted to adjust the microstructure of Bi<sub>2</sub>WO<sub>6</sub>. By using CTAB and PVP surfactants, Guo et al. [11] prepared nanosheet-assembled Bi<sub>2</sub>WO<sub>6</sub> microspheres and investigated the growth mechanism of the assembled microspheres. When used for the degradation of Rh B under visible light, the degradation efficiency was 98% within 50 min. By adopting CTAB surfactant and the mixed solvent of ethyl alcohol and ethylene glycol, Bai et al. [12] synthesized Bi<sub>2</sub>WO<sub>6</sub> photocatalysts with abundant oxygen vacancies. The generation of oxygen vacancy enhanced the photogenerated carrier separation efficiency and visible light absorption ability, which resulted in superior photocatalytic activity for the degradation of ciprofloxacin, and the degradation rate reached 90% within 6 h. In addition, the CTAB-capped Bi<sub>2</sub>WO<sub>6</sub> photocatalyst was synthesized with flower-like structures [13]. The CTAB surfactant affected the microstructure, which facilitated the physical adsorption of Rh B dye and enhanced the photoactivity of the resulting product. Consequently, the 0.20CTAB-Bi<sub>2</sub>WO<sub>6</sub> sample degraded 100% Rh B within 120 min. By using the CTAB surfactant and an ethylene glycol-water mixed solvent, Zhou et al. [14] synthesized Bi<sub>2</sub>WO<sub>6</sub> and Au-decorated Bi<sub>2</sub>WO<sub>6</sub> hollow microspheres. When used for the degradation of phenol under visible light, Au nanoparticle-decorated Bi<sub>2</sub>WO<sub>6</sub> delivered enhanced photocatalytic activity due to the cooperative electron trapping abilities and the SPR effect of Au nanoparticles.

### 2.3. Heteroatom Doping

Heteroatom doping can be adopted to adjust the crystal plane structure of Bi<sub>2</sub>WO<sub>6</sub> and broaden the light absorption range, which is widely reported to enhance the photoactivity of Bi<sub>2</sub>WO<sub>6</sub>. In this section, we summarize the advances of non-metal-doped Bi<sub>2</sub>WO<sub>6</sub> and metal-doped Bi<sub>2</sub>WO<sub>6</sub>.

In the existing non-metal dopants, N, F, Cl, and I serve as dopants for fabricating non-metal-doped Bi<sub>2</sub>WO<sub>6</sub> photocatalysts, and the major topics mostly involve the influence of the doping amount on the microstructures and photodegradation performance. In this respect, Hoang et al. [15] synthesized N-doped Bi<sub>2</sub>WO<sub>6</sub> nanoparticles and discussed the influence of the N-doping amount on photocatalytic activity. Through a comparison, the doped sample with a N/Bi atomic ratio of 0.5% presented the best photodegradation performance for removing Rh B under the irradiation of visible light. Chen et al. [16] prepared F-doped Bi<sub>2</sub>WO<sub>6</sub> via a hydrothermal route and investigated the effect of the F-doping amount on the sample morphology and degradation performance. With an increase of the F-doping amount, ultrathin Bi<sub>2</sub>WO<sub>6</sub> nanosheets were transformed into hierarchical

nanoflowers. When used for the degradation of tetracycline (TC), the degradation rate constant of the optimized F-BWO4 sample was about 4.5 times higher than that of pristine  $\text{Bi}_2\text{WO}_6$  due to the hierarchical structure and strong electronegativity. Phuruangrat et al. [17] reported the preparation of I-doped  $\text{Bi}_2\text{WO}_6$  photocatalysts and their degradation performance. The results showed that 3 wt% I-doped  $\text{Bi}_2\text{WO}_6$  presented the best performance, which degraded 100% Rh B in 100 min under the radiation of visible light, with a degradation rate of  $0.044 \text{ min}^{-1}$ .

Compared to non-metal doping, there are abundant works about metal-doped  $\text{Bi}_2\text{WO}_6$ , including Fe, Ti, Sr, Er, La, Au, Ag, and Mo dopants. Besides mono-metal doping, dual-metal doping was reported to further improve the photocatalytic activity of  $\text{Bi}_2\text{WO}_6$ . Among various metal dopants, the incorporation of Fe dopants would accelerate the electron-hole separation and improve the photocatalytic activity. In respect of the Fe-doping mechanism, Hu et al. [18] confirmed that Fe doping narrowed the energy band gap and induced abundant oxygen vacancies, which enhanced the separation efficiency of photogenerated carriers and the light absorption capability. When used for the degradation of Rh B and salicylic acid (SA), the optimized BW-Fe-0.10 sample showed 11.9 and 8.0 times higher than that of pristine  $\text{Bi}_2\text{WO}_6$ , respectively. Arif et al. [19] prepared Ti-doped  $\text{Bi}_2\text{WO}_6$  photocatalysts and confirmed that the presence of  $\text{Ti}^{3+}/\text{Ti}^{4+}$  in Ti-doped  $\text{Bi}_2\text{WO}_6$  promoted the generation of reactive oxygen species, which greatly enhanced the photocatalytic activity of  $\text{Bi}_2\text{WO}_6$ . Furthermore, the layered 3D hierarchical structure adjusted the band structure of  $\text{Bi}_2\text{WO}_6$ , further facilitating the enhancement of the photocatalytic performance. Maniyazagan et al. [20] synthesized hierarchical Sr- $\text{Bi}_2\text{WO}_6$  photocatalysts for the degradation of 4-NP and MB. As shown in Figure 2a, by optimizing the content of  $\text{Sr}^{2+}$  ions, the composite of 15% Sr- $\text{Bi}_2\text{WO}_6$  delivered the highest photocatalytic activity. Under the irradiation of UV light with  $\text{NaBH}_4$ , the optimized sample degraded 99.5% MB in 25 min and 99.4% 4-NP reduction in 15 min, respectively. The major reason was the enhanced charge carrier separation and the generation of oxygen vacancies. Qiu et al. [21] fabricated an  $\text{Er}^{3+}$ -mixed  $\text{Bi}_2\text{WO}_6$  photocatalyst by a one-step hydrothermal route (Figure 2b). After adding  $\text{Er}^{3+}$  ions,  $\text{Bi}_2\text{WO}_6$  was transformed into a layered nanosheet with a high specific surface area. The sample of 16%  $\text{Er}^{3+}$ - $\text{Bi}_2\text{WO}_6$  presented a high degradation rate of 94.58% TC within 60 min. The enhanced activity was attributed to the porous structure and enhanced separation efficiency of photogenerated electrons. Ning et al. [22] synthesized  $\text{La}^{3+}$ -doped  $\text{Bi}_2\text{WO}_6$  nanoplates for the degradation of Rh B. Compared to  $\text{Bi}_2\text{WO}_6$ , the doped sample showed a higher specific surface area, and the band gap reduced to 2.81 eV from 2.89 eV. Furthermore, the  $\text{La}^{3+}$ -doping enhanced the separation efficiency of electron and hole pairs. Therefore, the  $\text{La}^{3+}$ -doped  $\text{Bi}_2\text{WO}_6$  presented a higher degradation rate constant than pure  $\text{Bi}_2\text{WO}_6$ .

In respect of noble metal dopants, Phuruangrat et al. [23] synthesized Au-doped  $\text{Bi}_2\text{WO}_6$  and incorporated  $\text{Au}^{3+}$  ions into  $\text{Bi}_2\text{WO}_6$  lattice. By adjusting the doping amount of Au, 3% Au-doped  $\text{Bi}_2\text{WO}_6$  nanoplates presented the highest Rh B degradation rate of 96.25% within 240 min, which was 2.15 times higher than that of pure  $\text{Bi}_2\text{WO}_6$ . The superior performance was ascribed to the enhanced separation efficiency of photogenerated electrons and holes. In another work, Phu et al. [24] discussed the photocatalytic activities of Ag-doped  $\text{Bi}_2\text{WO}_6$  and Ag nanoparticle-decorated  $\text{Bi}_2\text{WO}_6$ . For Ag-doped sample, Ag ions substituted the lattice of  $\text{Bi}_2\text{WO}_6$ , while, for the decorated sample, abundant Ag nanoparticles were dispersed on the surface of  $\text{Bi}_2\text{WO}_6$  nanoparticles with no lattice change. When used for the degradation of Rh B by visible light, the activity of the Ag nanoparticles-modified sample was more than two times higher than that of the Ag-doped sample due to the enhanced surface plasmon resonance caused by Ag nanoparticles. Besides mono-metal doping, (La, Mo) co-doped  $\text{Bi}_2\text{WO}_6$  was reported [25]. The introduction of La and Mo adjusted the particle size and lattice spacing of  $\text{Bi}_2\text{WO}_6$ . Moreover, the La and Mo copopants inhibited the charge recombination. Consequently, the (0.25La, 0.25Mo)- $\text{Bi}_2\text{WO}_6$  sample containing 0.25 mol% La and 0.25 mol% Mo showed the highest activity for the photodegradation of MB.

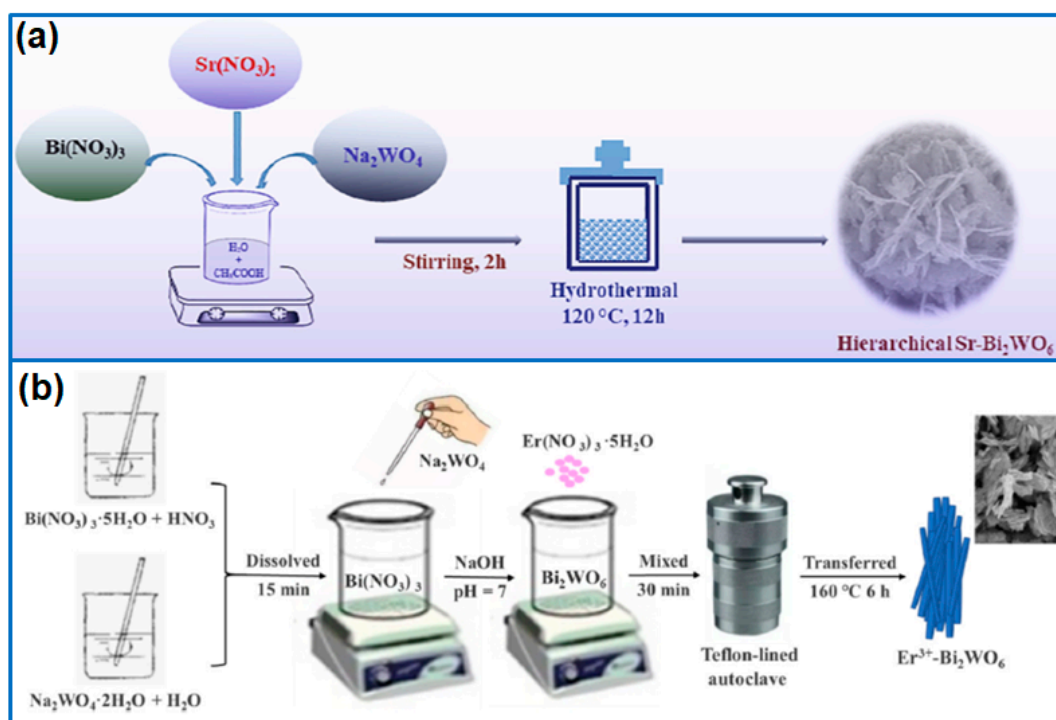


**Figure 2.** Fabrication process of (a) hierarchical Sr-Bi<sub>2</sub>WO<sub>6</sub> [20]. Copyright (2022) Elsevier. (b) Er<sup>3+</sup>-Bi<sub>2</sub>WO<sub>6</sub> photocatalyst [21]. Copyright (2022) Elsevier.

### 3. Bi<sub>2</sub>WO<sub>6</sub>-Based Binary Composite

Besides the decoration or doping of Bi<sub>2</sub>WO<sub>6</sub>, the construction of Bi<sub>2</sub>WO<sub>6</sub>-based composite is widely reported for enhancing the photoactivity of Bi<sub>2</sub>WO<sub>6</sub>. According to the type of candidate materials, we classified the existing Bi<sub>2</sub>WO<sub>6</sub>-based binary composites into six types: Bi<sub>2</sub>WO<sub>6</sub>/carbon or MOF composite, Bi<sub>2</sub>WO<sub>6</sub>/g-C<sub>3</sub>N<sub>4</sub> composite, Bi<sub>2</sub>WO<sub>6</sub>/metal oxides composite, Bi<sub>2</sub>WO<sub>6</sub>/metal sulfides composite, Bi<sub>2</sub>WO<sub>6</sub>/Bi-series composite, and Bi<sub>2</sub>WO<sub>6</sub>/metal tungstates composite. The design idea, microstructure, and photocatalytic performance of these binary composite photocatalysts are summarized in detail.

#### 3.1. Bi<sub>2</sub>WO<sub>6</sub>/Carbon or MOF Composite

Carbon materials exhibit good conductivity and a large specific surface area, which are more suitable for loading Bi<sub>2</sub>WO<sub>6</sub> nanostructures. In this section, various carbon materials, including graphene, carbon nanotube, carbon dots, and biomass-derived carbon are used for hybridizing with Bi<sub>2</sub>WO<sub>6</sub>. Among carbon materials, graphene oxide (GO) is a typical two-dimension template with abundant oxygen-containing groups, which can be served as ideal 2D substrates for loading semiconductors. Compared to GO, reduced GO (rGO) exhibits a superior electronic conductivity, which was adopted to hybridize with Bi<sub>2</sub>WO<sub>6</sub> to enhance the photodegradation efficiency. For example, Zhao et al. [26] fabricated an rGO/Bi<sub>2</sub>WO<sub>6</sub> composite photocatalyst via the hydrothermal method, and the composite degraded 87.49% norfloxacin within 180 min. The photocatalytic activity was much higher than that of pure Bi<sub>2</sub>WO<sub>6</sub> due to the efficient charge separation and enhanced light-harvesting capacity. Arya et al. [27] also prepared an rGO-Bi<sub>2</sub>WO<sub>6</sub> heterostructure via hydrothermal route and investigated their photocatalytic activity for the removal of levofloxacin. When kept in visible light at room temperature, the rGO-Bi<sub>2</sub>WO<sub>6</sub> composite achieved a high degradation rate of 74.3% within 120 min due to the inhibition of charge carrier recombination. Furthermore, multi-walled carbon nanotubes (MWNTs) were coupled with Bi<sub>2</sub>WO<sub>6</sub> to fabricate 3D mesoporous MWNTs-Bi<sub>2</sub>WO<sub>6</sub> microspheres [28]. The MWNTs promoted the transfer and separation of hole and electron pairs, which enhanced the light absorption capability of Bi<sub>2</sub>WO<sub>6</sub>. The composite containing 3% MWNTs showed the optimum photoactivity, and the degradation

efficiency was 1.35 times higher than that of pure  $\text{Bi}_2\text{WO}_6$ . In addition, carbon dots (CDs) were used for decorating a 3D Cl-doped  $\text{Bi}_2\text{WO}_6$  hollow microsphere to construct CDs/Cl- $\text{Bi}_2\text{WO}_6$  composite photocatalysts [29]. The introduced CDs and Cl doping enhanced the visible light absorption capability and inhibited the recombination of electron–hole pairs. The optimized 0.5% CDs/Cl- $\text{Bi}_2\text{WO}_6$  composite degraded 85.1% TCH within 60 min, which was much better than  $\text{Bi}_2\text{WO}_6$  and Cl- $\text{Bi}_2\text{WO}_6$ .

In addition, biomass-derived carbon materials were coupled with  $\text{Bi}_2\text{WO}_6$  to fabricate  $\text{Bi}_2\text{WO}_6/\text{C}$  hybrid photocatalysts. In this respect, Liang et al. [30] firstly prepared bamboo leave-derived carbon and then fabricated 3D flower-like  $\text{Bi}_2\text{WO}_6/\text{C}$  composites by hydrothermal route. The large specific surface area of biomass carbon enhanced the adsorption capacity; meanwhile, the good conductivity promoted the separation of charge carriers. The optimized  $\text{Bi}_2\text{WO}_6/\text{C}$  (6: 1) sample had a high degradation rate of 85.4% for the removal of TC within 90 min. Wang et al. [31] prepared a  $\text{Bi}_2\text{WO}_6/\text{N}$ -modified biochar (BW/N-B) composite for the degradation of Rh B pollutant. The loading of N-B improved the photocatalytic activity due to the enhanced separation and transfer of electron–hole pairs. Under the irradiation of visible light, the BW/N1-B sample with a urea/biochar ratio of 2:1 presented the best photocatalytic activity, which degraded 99.1% Rh B within 45 min. In addition, N and S co-doped corn straw biochar (NSBC) was used to hybridize with  $\text{Bi}_2\text{WO}_6$  to form  $\text{Bi}_2\text{WO}_6/\text{NSBC}$  composite photocatalysts (Figure 3a) for the degradation of ciprofloxacin (CIP) [32]. The N and S co-doped biochar exhibited a high specific surface area and interconnected fiber structure and high catalytic property, which effectively prevented the agglomeration of  $\text{Bi}_2\text{WO}_6$ . The combination of NSBC and  $\text{Bi}_2\text{WO}_6$  extended the visible light response, adjusted the band gap, and promoted the separation and transfer of photoinduced carriers, which achieved the fast degradation of CIP (5 mg/L) within 75 min.

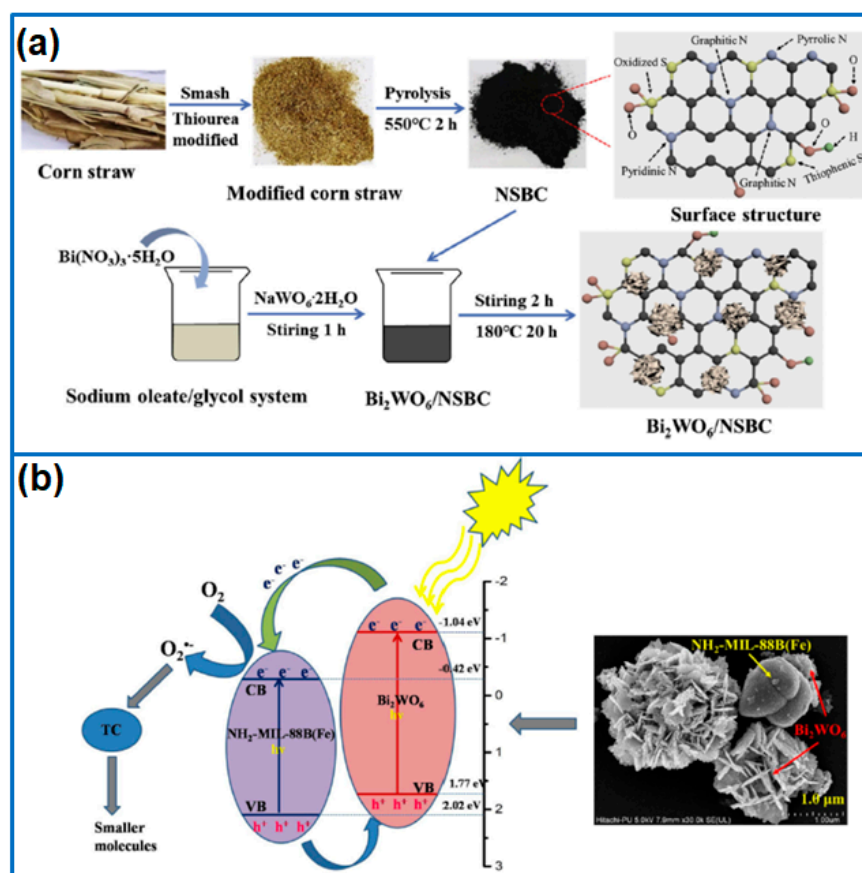


**Figure 3.** Preparation of (a)  $\text{Bi}_2\text{WO}_6/\text{NSBC}$  composite [32]. Copyright (2021) Elsevier. (b)  $\text{Bi}_2\text{WO}_6/\text{NH}_2\text{-MIL-88B(Fe)}$  heterostructure [33]. Copyright (2021) Elsevier.

Metal-organic frameworks (MOFs) consist of metal ions or metal clusters and organic ligands, which show some advantages in permanent porosity, tunable pore size, high specific surface area, and active surface chemistry. Various MOFs are widely utilized in adsorption, gas storage and separation, energy storage, and photocatalysis. In the field of photocatalysis, various MOFs, including Fe-based MOFs and Zn-based MOFs, are coupled with  $\text{Bi}_2\text{WO}_6$  to fabricate hybrid photocatalysts. In this respect, MIL-100(Fe) nanoparticles were hybridized with  $\text{Bi}_2\text{WO}_6$  nanosheets to construct MIL-100(Fe)/ $\text{Bi}_2\text{WO}_6$  Z-scheme heterojunction [34]. When tested for the degradation of TC under sunlight, the optimized 12% MIL/BWO delivered the highest photocatalytic activity due to the large specific surface area, enhanced light adsorption range, and high charge transfer and separation efficiency. In addition, the MIL-88A(Fe)/ $\text{Bi}_2\text{WO}_6$  heterojunction was synthesized for the degradation of Rh B and TC [35]. The combination of MIL-88A(Fe) and  $\text{Bi}_2\text{WO}_6$  effectively inhibited the recombination of photogenerated carriers. Under the irradiation of visible light, the heterojunction degraded 96% Rh B and 71% TC within 50 min and 80 min, respectively. Kaur et al. [33] prepared a  $\text{Bi}_2\text{WO}_6/\text{NH}_2\text{-MIL-88B(Fe)}$  heterostructure for the degradation of TC (Figure 3b). Due to the promoted separation and transfer of photoexcited charges caused by the interfacial contact, the heterostructure presented a high degradation efficiency of 89.4% within 130 min under solar illumination. Tu et al. [36] synthesized MIL-53(Fe)/ $\text{Bi}_2\text{WO}_6$  heterostructure photocatalysts. The formation of heterojunction extended the visible light absorption capability and accelerated the transfer of photogenerated electrons. When used for the degradation of Rh B and phenol Rh B under visible light irradiation, the degradation rate constants of the heterostructure containing 5 wt% MIL-53(Fe) were 3.75-fold and 3.27-fold higher than that of pristine  $\text{Bi}_2\text{WO}_6$ .

Besides various Fe-based MOFs, Zhang et al. [37] prepared hydrangea-like  $\text{Bi}_2\text{WO}_6/\text{ZIF-8}$  (BWOZ) hybrid photocatalysts by using a flower-like  $\text{Bi}_2\text{WO}_6$  template. The generation of heterojunction induced the fast separation of photogenerated carriers. Meanwhile, the optimized BWOZ containing 7.0 wt%  $\text{Bi}_2\text{WO}_6$  showed a large specific surface area, which degraded 85.7% MB within 240 min, and the reaction kinetic constant was 23-fold and 1.61-fold higher than that of pure  $\text{Bi}_2\text{WO}_6$  and ZIF-8, respectively. In addition, Dai et al. [38] also fabricated  $\text{Bi}_2\text{WO}_6/\text{ZIF-8}$  composite photocatalysts for the degradation of TC. Under the irradiation of UV light, the optimized sample achieved the fast degradation of 97.8% TC (20 mg/L) within 80 min, and the degradation rate constant was about 3-fold higher than that of pure  $\text{Bi}_2\text{WO}_6$ .

### 3.2. $\text{Bi}_2\text{WO}_6/\text{g-C}_3\text{N}_4$ Composite

Serving as a non-metal semiconductor, graphitic carbon nitride ( $\text{g-C}_3\text{N}_4$ ) presents two-dimensional graphite-like structures with a high specific surface area, which are widely adopted as active templates for loading various semiconductor photocatalysts. In this section, we introduce the research progress of  $\text{Bi}_2\text{WO}_6/\text{g-C}_3\text{N}_4$  composite photocatalysts. Qi et al. [39] prepared  $\text{Bi}_2\text{WO}_6/\text{g-C}_3\text{N}_4$  heterojunction by hydrothermal reaction and discussed the effect of  $\text{g-C}_3\text{N}_4/\text{Bi}_2\text{WO}_6$  ratio on photodegradation performance. When the  $\text{Bi}_2\text{WO}_6$  ratio was 10 wt%, the composite presented the highest photocatalytic activity for the degradation of MB, and the reaction rate constant was 4 and 1.94 times higher than that of pristine  $\text{g-C}_3\text{N}_4$  and  $\text{Bi}_2\text{WO}_6$ , respectively. In addition, Zhao et al. [40] also prepared  $\text{Bi}_2\text{WO}_6/\text{g-C}_3\text{N}_4$  (BW/CNNs, Figure 4a) composite photocatalysts for the degradation of Ceftriaxone sodium in an aquatic environment. The combination of the two components enhanced the absorption capability of visible light and accelerated the separation of photogenerated electron-hole pairs. As a result, the 40%-BW/CNNs delivered the best photocatalytic activity, which degraded 94.50% Ceftriaxone sodium within 120 min under the irradiation of visible light. Chen et al. [41] synthesized  $\text{Bi}_2\text{WO}_6$  on  $\text{g-C}_3\text{N}_4$  to fabricate  $\text{Bi}_2\text{WO}_6/\text{g-C}_3\text{N}_4$  heterojunctions by a hydrothermal route. When used for the degradation of Rh B and phenol solution, the composite with a Bi/ $\text{g-C}_3\text{N}_4$  molar ratio of 4% presented the highest photodegradation activity for the highest separation efficiency of

photogenerated electron–hole pairs. Moreover, the separation and transfer of electron–hole pairs were proven as a direct Z-scheme mechanism.

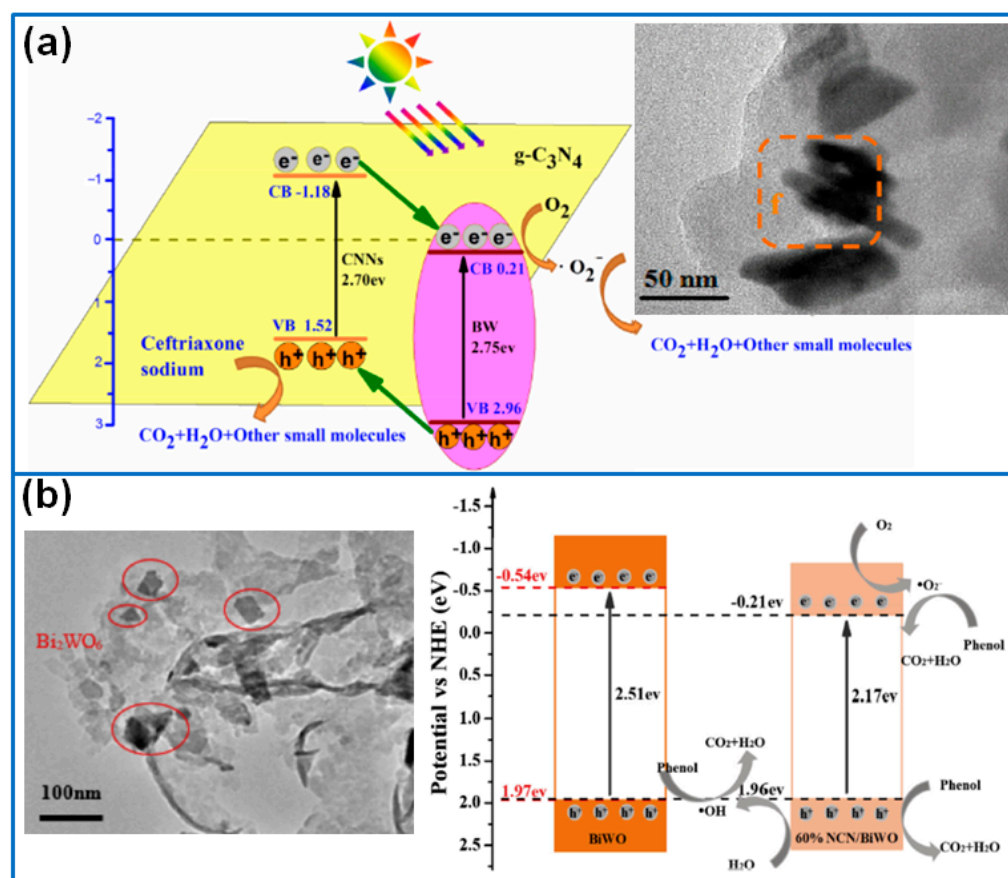


**Figure 4.** Photocatalytic mechanism of (a)  $\text{Bi}_2\text{WO}_6/\text{g-C}_3\text{N}_4$  [40]. Copyright (2018) Elsevier. (b) N-doped  $\text{g-C}_3\text{N}_4$  (NCN)/ $\text{Bi}_2\text{WO}_6$  [42]. Copyright (2020) Elsevier.

In respect of the microstructure design, Zhu et al. [42] prepared various N-doped  $\text{g-C}_3\text{N}_4$  (NCN)/ $\text{Bi}_2\text{WO}_6$  (BWO) composites by using NCN as the template, as shown in Figure 4b. The ratio of NCN/BWO was adjusted to reduce the band gap and increase the surface area. The 60% NCN/BWO presented the best photocatalytic activity, which achieved the fast degradation of 93.1% phenol within 5 h, and the degradation rate constant was 18.5 times higher than that of  $\text{Bi}_2\text{WO}_6$ . The major reason was ascribed to the enhanced visible light absorption capability caused by NCN. Wang et al. [43] prepared core-shell structured  $\text{g-C}_3\text{N}_4@\text{Bi}_2\text{WO}_6$  composite by in situ, forming an ultrathin  $\text{g-C}_3\text{N}_4$  shell layer on  $\text{Bi}_2\text{WO}_6$  nanosheets. By adjusting the thickness of the  $\text{g-C}_3\text{N}_4$  shell layer, the interface of  $\text{g-C}_3\text{N}_4@\text{Bi}_2\text{WO}_6$  was optimized to promote the separation efficiency of photogenerated electron–hole pairs. As a result, the composite photocatalyst with a 1 nm-thick shell layer delivered the optimum degradation phenol activity under visible light, which was about 1.9 times higher than that of  $\text{Bi}_2\text{WO}_6$  and 5.7 times higher than that of  $\text{g-C}_3\text{N}_4$ . Zhang et al. [44] prepared  $\text{g-C}_3\text{N}_4$  quantum dot (CNQD)-decorated ultrathin  $\text{Bi}_2\text{WO}_6$  nanosheets for the degradation of Rh B and tetracycline (TC) under the irradiation of visible light. By optimizing the ratio, the composite of 5% CNQDs/BWO delivered the highest photocatalytic performance, which degraded 87% TC and 92.51% Rh B within 60 min. The superior activity can be ascribed to the Z-scheme charge transfer mechanism, the up-conversion behavior of CNQDs, and the enhanced separation and transfer rates of photo-generated charges. Regarding the performance of different S-scheme heterojunctions, Gordanshekan et al. [45] compared the photocatalytic activity of  $\text{Bi}_2\text{WO}_6/\text{g-C}_3\text{N}_4$  with  $\text{Bi}_2\text{WO}_6/\text{TiO}_2$ . When serving as photocatalysts for removing cefixime (CFX) in polluted



water,  $\text{Bi}_2\text{WO}_6/\text{g-C}_3\text{N}_4$  showed a removal efficiency of 94%, which was slightly higher than that of  $\text{Bi}_2\text{WO}_6/\text{TiO}_2$  (91%).

### 3.3. $\text{Bi}_2\text{WO}_6/\text{Metal Oxides Composite}$

Metal oxides have a wide range, and most of them can serve as semiconductor photocatalysts. To further enhance the photoactivity of  $\text{Bi}_2\text{WO}_6$ , various metal oxide semiconductors, including  $\text{TiO}_2$ ,  $\text{ZnO}$ , and other metal oxides, are reported to hybridize with  $\text{Bi}_2\text{WO}_6$ , and the research progress of  $\text{Bi}_2\text{WO}_6/\text{metal oxides}$  composites is introduced in this section.

#### 3.3.1. $\text{Bi}_2\text{WO}_6/\text{TiO}_2$ Composite

Compared to other metal oxides,  $\text{TiO}_2$  exhibits some advantages of low cost, low toxicity, strong redox ability, and high catalytic activity, and it is regarded as the most popular photocatalyst in the past few decades. However, the wide band gap of 3.0–3.2 eV limits the visible light adsorption, only allowing a UV light response. Moreover, the fast recombination of photogenerated electron–hole pairs further weakens the photocatalytic activity of  $\text{TiO}_2$ . The combination of  $\text{TiO}_2$  with  $\text{Bi}_2\text{WO}_6$  overcomes the shortage of  $\text{TiO}_2$ , and various  $\text{TiO}_2/\text{Bi}_2\text{WO}_6$  composite photocatalysts were developed in recent years. For example, Li et al. [46] fabricated  $\text{TiO}_2/\text{Bi}_2\text{WO}_6$  microflowers via a one-step hydrothermal reaction, in which  $\text{TiO}_2$  nanoparticles (10 nm) were dispersed on  $\text{Bi}_2\text{WO}_6$  microflowers. The  $\text{TiO}_2/\text{Bi}_2\text{WO}_6$  composite degraded 100% Rh B within 60 min under visible light or 30 min under UV-vis light. The enhanced photocatalytic activity was ascribed to the synergistic effect of two components. Furthermore, the improved light adsorption capacity and carrier separation efficiency also facilitated the photoactivity. In addition, an electrospinning technique was adopted to fabricate  $\text{Bi}_2\text{WO}_6/\text{TiO}_2$  nanofibers (BTNF) by decorating  $\text{Bi}_2\text{WO}_6$  nanosheets on the  $\text{TiO}_2$  fiber surface [47]. In this composite, the  $\text{Bi}_2\text{WO}_6$  extended the light absorption range, and the  $\text{Bi}_2\text{WO}_6/\text{TiO}_2$  heterojunction promoted the charge separation. Therefore, BTNF presented a superior visible light activity for degrading Rh B, which was much better than pure  $\text{Bi}_2\text{WO}_6$ ,  $\text{TiO}_2$ , and their mixture. Lu et al. [48] deposited  $\text{Bi}_2\text{WO}_6$  nanosheets onto  $\text{TiO}_2$  nanotube arrays (TNTAs) to fabricate BWO/TNTAs composite photocatalysts. The 0.2BWO/TNTAs sample achieved the fast degradation of 92.2% TC within 180 min due to the promoted charge separation and extended light absorption range.

Besides the direct combination of  $\text{Bi}_2\text{WO}_6$  and  $\text{TiO}_2$ , Wang et al. [49] prepared  $\text{Sb}^{3+}$  doped  $\text{Bi}_2\text{WO}_6/\text{TiO}_2$  nanotube photocatalysts. A rose-like BWO-10 sample showed superior photocatalytic activity, which achieved the fast degradation of 80.58% Rh B, 77.23% MO, and 99.06% MB under the irradiation of visible light, and the best performance resulted from the uniform rose-like structure and adjusted energy level. Sun et al. [50] prepared N/ $\text{Ti}^{3+}$  co-doped  $\text{TiO}_2/\text{Bi}_2\text{WO}_6$  heterojunctions (NT-TBWx) and proved that the degradation rate order of organic pollutants was photocatalysis < sonocatalysis < sonophotocatalysis. The superior performance was attributed to the doping level, heterophase junction, and heterojunction.

#### 3.3.2. $\text{Bi}_2\text{WO}_6/\text{ZnO}$ Composite

To achieve the combination of narrow-band gap  $\text{Bi}_2\text{WO}_6$  and wide-band gap  $\text{ZnO}$ , various  $\text{ZnO}/\text{Bi}_2\text{WO}_6$  (ZBW) heterostructures were developed to improve the photocatalytic activity of  $\text{Bi}_2\text{WO}_6$ . In this respect, Liu et al. [51] synthesized the ZBW heterostructure via the hydrothermal method and investigated the photocatalytic activity for degrading MB under ultraviolet light. ZBW degraded 95.48% MB within 120 min, and the excellent photocatalytic performance was due to the promoted separation of electrons and holes caused by the heterojunction. Koutavarapu et al. [52] synthesized a hetero-structured  $\text{Bi}_2\text{WO}_6/\text{ZnO}$  composite via a hydrothermal route for the degradation of Rh B under solar irradiation. The formation of a  $\text{Bi}_2\text{WO}_6/\text{ZnO}$  interface reduced the charge transfer resistance and inhibited the recombination of charge carriers. By adjusting the additional amount of  $\text{ZnO}$ , the optimized BWZ-20 composite showed the best photocatalytic activity, which degraded 99% Rh B within 50 min. Chen et al. [53] synthesized a  $\text{ZnO}/\text{Bi}_2\text{WO}_6$  heterostructure on flexible

carbon cloth (CC) substrate. The optimized Z3B-CC sample containing 3 wt%  $\text{Bi}_2\text{WO}_6$  degraded 96.9% MB within 100 min, which also facilitated the reuse of the photocatalyst. The enhanced activity was related to the enhanced light absorption range and the formation of a type-II energy band structure. To further enhance the activity, Zhao et al. [54] prepared a Z-scheme C and N-co-doped  $\text{ZnO}/\text{Bi}_2\text{WO}_6$  (CZB) hybrid photocatalyst, and the influence of the C and N-co-doped  $\text{ZnO}$  content on the photodegradation performance of CZB composites was investigated. In this complicated structure, C and N co-doping adjusted the energy level and enhanced light absorption. Furthermore, residual C accelerated the separation and transfer of photogenerated carries. Through a comparison, CZB containing 5 wt% C/N- $\text{ZnO}$  presented the best activity for the removal of tetracycline, enrofloxacin, and norfloxacin under visible light, and the photodegradation mechanism was confirmed as the formation of a Z-scheme heterojunction.

### 3.3.3. $\text{Bi}_2\text{WO}_6$ /Other Metal Oxides Composite

Besides commonly used  $\text{TiO}_2$  and  $\text{ZnO}$ , other metal oxides, including  $\text{SnO}_2$ ,  $\text{MnO}_2$ ,  $\text{Co}_3\text{O}_4$ ,  $\text{Fe}_3\text{O}_4$ ,  $\text{CuO}$ ,  $\text{WO}_3$ ,  $\text{Bi}_2\text{O}_4$ , and  $\text{In}_2\text{O}_3$ , were hybridized with  $\text{Bi}_2\text{WO}_6$  to enhance photocatalytic activity. For example, Salari et al. [55] prepared Z-scheme flower-like  $\text{Bi}_2\text{WO}_6/\text{MnO}_2$  composite photocatalysts, in which  $\text{MnO}_2$  nanoparticles that were dispersed on 3D  $\text{Bi}_2\text{WO}_6$  flowers enhanced the transfer and separation of charge carriers. As a result, the optimized  $\text{Bi}_2\text{WO}_6/\text{MnO}_2$  (1:10) degraded 100% MB within 100 min. Mallikarjuna et al. [56] deposited small  $\text{SnO}_2$  nanoparticles onto  $\text{Bi}_2\text{WO}_6$  nanoplates to fabricate  $\text{SnO}_2/2\text{D-Bi}_2\text{WO}_6$  photocatalysts (Figure 5a). The loading of  $\text{SnO}_2$  nanoparticles adjusted the visible light absorption region and promoted charge separation and transfer efficiency. When used for degrading the Rh B pollutant, the photocatalytic activity of the composite was more than 2.7 times higher than that of 2D- $\text{Bi}_2\text{WO}_6$  nanoplates.

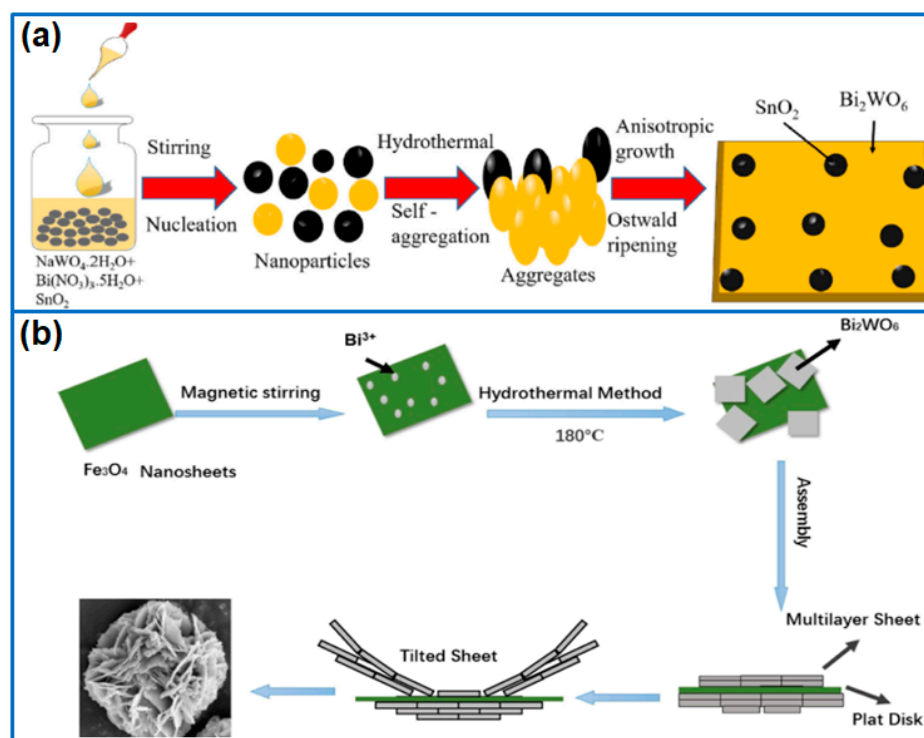


**Figure 5.** Fabrication process of (a)  $\text{SnO}_2/2\text{D-Bi}_2\text{WO}_6$  [56]. Copyright (2021) Elsevier. (b)  $\text{Fe}_3\text{O}_4/\text{Bi}_2\text{WO}_6$  heterojunction [57]. Copyright (2021) American Chemical Society.

Zhang et al. [58] prepared flower-like  $\text{Co}_3\text{O}_4$  QDs/ $\text{Bi}_2\text{WO}_6$  composite photocatalysts to achieve the uniform dispersion of  $\text{Co}_3\text{O}_4$  QDs on flower-like nanosheets. By adjusting the ratio of  $\text{Co}_3\text{O}_4$  QDs, the sample of 10%- $\text{Co}_3\text{O}_4$  QDs/ $\text{Bi}_2\text{WO}_6$  presented the optimum

performance for the removal of TC, and the degradation rate constant was about 1.55 and 3.40 times higher than that of  $\text{Bi}_2\text{WO}_6$  and  $\text{Co}_3\text{O}_4$  QDs, respectively. The superior performance was ascribed to the formation of a p–n heterojunction and enhanced the visible light absorption capacity. Zhu et al. [57] prepared Z-scheme  $\text{Fe}_3\text{O}_4/\text{Bi}_2\text{WO}_6$  heterojunctions as photocatalysts for degrading ciprofloxacin (CIP), in which the flower-like composite was assembled by abundant nanosheets (Figure 5b). The formation of Z-scheme heterojunctions facilitated the light-harvesting capacity and suppressed the recombination of photogenerated carriers. Under the irradiation of visible light, the FB-180 sample prepared at 180 °C with 4% Fe delivered optimum photoactivity, which degraded about 99.7% CIP within 15 min. Moreover, the sample showed superior reusability and stability. Koutavarapu et al. [59] fabricated  $\text{CuO}/\text{Bi}_2\text{WO}_6$  (CuBW) composite photocatalysts for degrading TC and MB. In this composite,  $\text{Bi}_2\text{WO}_6$  provided transfer pathways for photogenerated electrons, while CuO was used to receive carriers from  $\text{Bi}_2\text{WO}_6$  and inhibited the recombination of charge carriers; thus, the formation of the heterostructure improved the photocatalytic activity. The optimized CuBW sample containing 10 mg  $\text{Bi}_2\text{WO}_6$  showed the highest degradation efficiency, which degraded 97.72% TC within 75 min and 99.43% MB within 45 min.

In respect of interface engineering design, Chen et al. [60] achieved the in-situ growth of (001)- and (110)-exposed  $\text{WO}_3$  on (010)-exposed  $\text{Bi}_2\text{WO}_6$  to form Z-scheme heterojunction photocatalysts. The facet control produced some dislocation defects for promoting the carriers transfer. Furthermore, Z-scheme transfer mode optimized the transfer of photogenerated electrons and improved the oxidization ability of photogenerated holes. Consequently, the  $\text{WO}_3$  (001) and (110)/ $\text{Bi}_2\text{WO}_6$  achieved a high removal rate of 74.5% for salicylic acid within 6 h, and the kinetic constant was 2.4 times higher than that of  $\text{WO}_3$  (001)/ $\text{Bi}_2\text{WO}_6$ .

In addition,  $\text{Bi}_2\text{O}_4$  micro-rods were in situ grown on  $\text{Bi}_2\text{WO}_6$  microspheres to form a  $\text{Bi}_2\text{O}_4/\text{Bi}_2\text{WO}_6$  heterojunction [61]. The heterojunction facilitated the separation and transfer of charge carriers. When used for the degradation of Rh B under visible light, the degradation rate constant of the composite was 5 times higher than that of pure  $\text{Bi}_2\text{WO}_6$ . While degrading MO, the enhanced factor reached 90-fold. Besides  $\text{Bi}_2\text{O}_4$ , a flower-like  $\text{Bi}_2\text{WO}_6/\text{Bi}_2\text{O}_3$  photocatalyst was also synthesized by the ionic liquid solvothermal method and calcination [62], and it presented a higher photocatalytic  $\text{H}_2$  production activity than pure  $\text{Bi}_2\text{WO}_6$ . Qin et al. [63] prepared a rich oxygen vacancy (OVs)  $\text{Bi}_2\text{WO}_6/\text{In}_2\text{O}_3$  hybrid photocatalyst for the degradation of Rh B. The formation of a  $\text{Bi}_2\text{WO}_6/\text{In}_2\text{O}_3$  heterostructure extended the lifetime of photogenerated charge carriers. Furthermore, the OVs in  $\text{Bi}_2\text{WO}_6/\text{In}_2\text{O}_3$  accelerated the separation of photogenerated electron–hole pairs. Through comparison, the BiIn80 sample containing 80 wt%  $\text{Bi}_2\text{WO}_6$  exhibited the best photocatalytic activity, and the reaction rate constant was about 4.17-fold and 15-fold higher than that of  $\text{Bi}_2\text{WO}_6$  and  $\text{In}_2\text{O}_3$ , respectively.

### 3.4. $\text{Bi}_2\text{WO}_6/\text{Metal Sulfides Composite}$

To effectively optimize the band edge of  $\text{Bi}_2\text{WO}_6$ , except for metal oxides, various metal sulfides were used to construct a  $\text{Bi}_2\text{WO}_6$ -containing Z-scheme heterojunction for enhancing visible light harvesting capability, such as,  $\text{Cu}_2\text{S}$ ,  $\text{MoS}_2$  or  $\text{MoSe}_2$ ,  $\text{SnS}_2$ ,  $\text{WS}_2$ ,  $\text{CdS}$ ,  $\text{Bi}_2\text{S}_3$ ,  $\text{In}_2\text{S}_3$ ,  $\text{CuInS}_2$ , and  $\text{FeInS}_4$ .

In this field, Tang et al. [64] prepared hierarchical flower-like  $\text{Cu}_2\text{S}/\text{Bi}_2\text{WO}_6$  photocatalysts via a three-step method, in which  $\text{Cu}_2\text{S}$  particles were distributed on the surface of  $\text{Bi}_2\text{WO}_6$  nanosheets (Figure 6a). Attributed to the hierarchical structure, the enhanced visible light absorption capacity, and the Z-scheme transfer mechanism, the sample of 1% $\text{Cu}_2\text{S}/\text{Bi}_2\text{WO}_6$  presented the highest photocatalytic activity for the removal of glyphosate. Based on the exfoliated  $\text{MoS}_2$  nanosheets as substrates, Zhang et al. [65] synthesized Z-scheme hetero-structured  $\text{MoS}_2/\text{Bi}_2\text{WO}_6$  hierarchical flower-like microspheres, in which the  $\text{MoS}_2$  substrate greatly affected the morphology and photocatalytic activity of the heterostructure (Figure 6b). The optimized composite degraded 100% Rh B within 90 min

and killed almost all of *Pseudomonas aeruginosa* within 60 min. Similar to  $\text{MoS}_2$ , layered  $\text{MoSe}_2/\text{Bi}_2\text{WO}_6$  composite photocatalysts were reported for the photocatalytic oxidation of gaseous toluene [66]. The formation of a p–n heterojunction provided a strong interlayer interaction, which effectively inhibited the recombination of photoinduced electron–hole pairs. The optimized 1.5%– $\text{MoSe}_2/\text{Bi}_2\text{WO}_6$  presented the highest activity, which degraded 80% gaseous toluene within 3 h under the irradiation of visible light, and the rate constant was about 7 times and 6 times higher than that of pure  $\text{MoSe}_2$  and  $\text{Bi}_2\text{WO}_6$ , respectively.

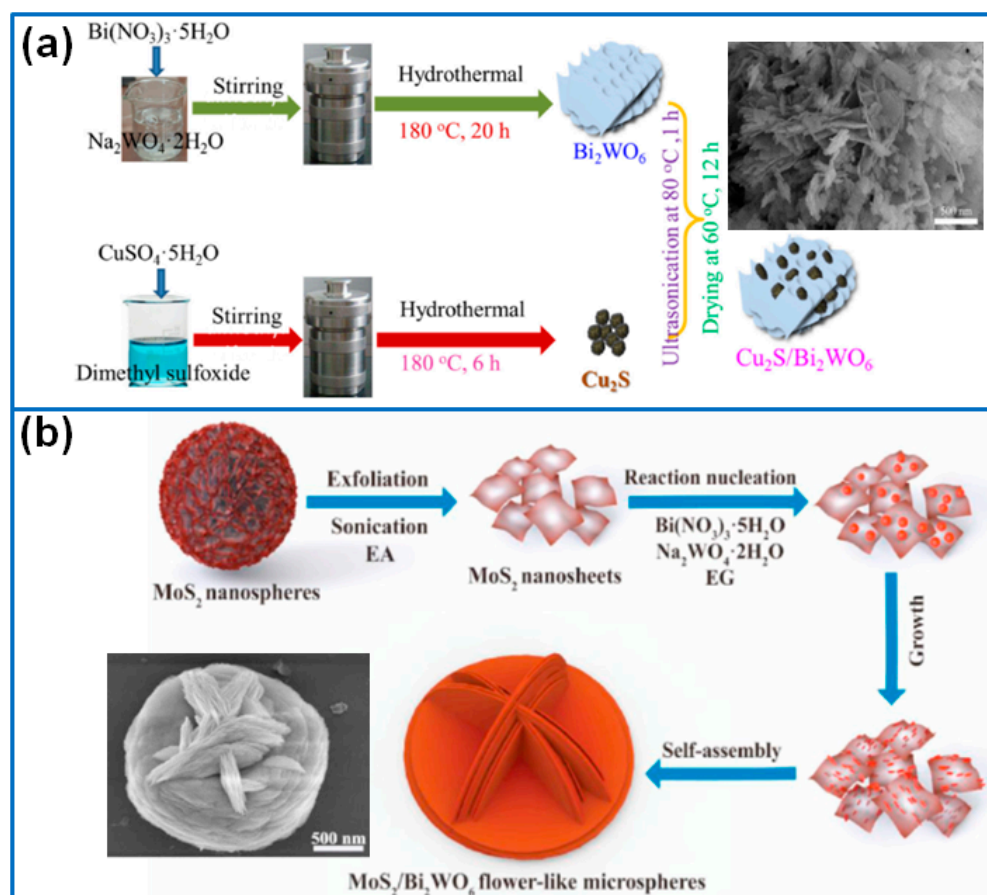


**Figure 6.** Fabrication process of (a) flower-like  $\text{Cu}_2\text{S}/\text{Bi}_2\text{WO}_6$  [64]. Copyright (2020) Elsevier. (b)  $\text{MoS}_2/\text{Bi}_2\text{WO}_6$  microspheres [65]. Copyright (2021) Elsevier.

Kumar et al. [67] synthesized a  $\text{SnS}_2/\text{Bi}_2\text{WO}_6$  plate-on-plate composite via a two-step hydrothermal route for the degradation of tetracycline (TC) and ciprofloxacin (CIP). Due to the formation of a Z-scheme heterojunction, the optimized 0.10 $\text{SnS}_2/\text{Bi}_2\text{WO}_6$  exhibited superior photocatalytic activity, which degraded 97% TC and 93% CIP within 90 min under sunlight exposure, and the degradation rate constant was three-fold higher than that of pure  $\text{Bi}_2\text{WO}_6$ . Similar to the plate-on-plate structure, Su et al. [68] synthesized an sTable 2D/2D  $\text{WS}_2/\text{Bi}_2\text{WO}_6$  heterostructure photocatalyst via a hydrothermal reaction. The generated Z-scheme heterostructure promoted the separation and transfer of photogenerated carriers, which showed much higher photocatalytic activity for the degradation of Rh B and OTC than pure  $\text{WS}_2$  or  $\text{Bi}_2\text{WO}_6$ .

Su et al. [69] synthesized CdS quantum dots (QDs) on a  $\text{Bi}_2\text{WO}_6$  monolayer via an in situ hydrothermal method to construct a S-scheme heterojunction. The Bi–S coordination at the junction interface enhanced the charge separation and interfacial charge migration. The optimized composite containing 7% CdS exhibited the best photocatalytic activity, which completely decomposed 100 ppm  $\text{C}_2\text{H}_4$  within 15 min, and the degradation rate constant was 88 times and 194 times higher than that of pure CdS and  $\text{Bi}_2\text{WO}_6$ . In addition,

CdS nanocrystals were decorated on the surface of  $\text{Bi}_2\text{WO}_6$  clusters to form  $\text{CdS@Bi}_2\text{WO}_6$  photocatalysts [70]. By adjusting the microstructure of CdS, the CdS nanorod-decorated  $\text{Bi}_2\text{WO}_6$  showed a higher charge separation capability than that of CdS cluster-decorated  $\text{Bi}_2\text{WO}_6$ , which degraded 96.1% Rh B within 120 min. Xu et al. [71] fabricated  $\text{Bi}_2\text{S}_3/2\text{D-Bi}_2\text{WO}_6$  composite photocatalysts by using the ion exchange method, in which the  $\text{Bi}_2\text{S}_3$  nanoparticle loading on  $\text{Bi}_2\text{WO}_6$  nanosheets enhanced the light absorption ability and promoted the transfer and separation of photogenerated carriers. The optimized BWS-2 sample achieved the complete degradation of Rh B much better than that of  $\text{Bi}_2\text{WO}_6$  nanosheets. He et al. [72] fabricated a core-shell structured  $\text{In}_2\text{S}_3/\text{Bi}_2\text{WO}_6$  composite by using  $\text{In}_2\text{S}_3$  microspheres as templates. The combination of the core and  $\text{Bi}_2\text{WO}_6$  shell extended the visible-light absorption range and enabled the Z-scheme transfer pathway. Therefore, the core-shell composite achieved the fast degradation of TCH, and the activity was 2.1 and 2.4 times higher than that of pure  $\text{Bi}_2\text{WO}_6$  and  $\text{In}_2\text{S}_3$ , respectively.

As important semiconductors,  $\text{CuInS}_2$  and  $\text{FeIn}_2\text{S}_4$  exhibit a strong light absorption capability, with suitable energy band edges, which serve as high-performance visible light photocatalysts in the photocatalytic field. Lu et al. [73] synthesized  $\text{Bi}_2\text{WO}_6$  on the surface of network-like  $\text{CuInS}_2$  microspheres to fabricate a Z-scheme  $\text{CuInS}_2/\text{Bi}_2\text{WO}_6$  heterojunction. The heterojunction interface enhanced the charge transfer capability, further promoting the separation of charge carriers. When used for the degradation of tetracycline hydrochloride (TCH), the activity of 15%  $\text{CuInS}_2/\text{Bi}_2\text{WO}_6$  was three-fold higher than that of pure  $\text{CuInS}_2$  and 17% higher than that of pure  $\text{Bi}_2\text{WO}_6$ . Shangguan et al. [74] prepared Z-scheme  $\text{FeIn}_2\text{S}_4/\text{Bi}_2\text{WO}_6$  composite photocatalysts for the degradation of TCH. The formation of a direct Z-scheme heterojunction promoted the separation of photogenerated holes and electrons, which presented enhanced activity for the removal of TCH, much better than pure  $\text{Bi}_2\text{WO}_6$  and  $\text{FeIn}_2\text{S}_4$ .

### 3.5. $\text{Bi}_2\text{WO}_6/\text{Bi}$ -Series Composite

Except for  $\text{Bi}_2\text{WO}_6$ , other Bi-containing semiconductors, including  $\text{BiOCl}$ ,  $\text{BiOBr}$ ,  $\text{BiOI}$ ,  $\text{Bi}_2\text{O}_2\text{CO}_3$ ,  $\text{BiPO}_4$ ,  $\text{Bi}_2\text{Sn}_2\text{O}_7$ ,  $\text{BiFeO}_3$ , and  $\text{CuBi}_2\text{O}_4$ , also exhibit excellent visible light adsorption capability and photocatalytic activity. The combination of  $\text{Bi}_2\text{WO}_6$  and other Bi-containing semiconductors can be regarded as an effective strategy for enhancing the photoactivity of  $\text{Bi}_2\text{WO}_6$ .

In this field, Guo et al. [75] synthesized  $\text{Bi}_2\text{WO}_6$  nanoparticles on layered  $\text{BiOCl}$  nanosheets to fabricate 0D/2D  $\text{Bi}_2\text{WO}_6/\text{BiOCl}$  composite photocatalysts. The formed heterojunction interface promoted the separation of photogenerated charge carriers. As a result, the optimized 1%  $\text{Bi}_2\text{WO}_6/\text{BiOCl}$  sample showed a superior degradation performance for removing OTC and phenol, and the degradation rate of OTC and phenol was 2.7-fold and 6.1-fold higher than that of pure  $\text{BiOCl}$ . Liang et al. [76] prepared a  $\text{Bi}_2\text{WO}_6/\text{BiOCl}$  heterojunction via the one-step hydrothermal method for the degradation of Rh B and TC. The formed heterojunction at the  $\text{Bi}_2\text{WO}_6/\text{BiOCl}$  interface promoted the separation of photogenerated electron-hole pairs, further improving the photocatalytic activity. Liu et al. [77] synthesized a 2D-3D  $\text{BiOBr}/\text{Bi}_2\text{WO}_6$  composite with 2D  $\text{Bi}_2\text{WO}_6$  nanosheets inserted in  $\text{BiOBr}$  microspheres. 3D  $\text{BiOBr}$  microspheres reduced the aggregation of  $\text{Bi}_2\text{WO}_6$  nanosheets and enhanced the visible light absorption capability by providing interfacial contact. Through optimization, the  $\text{BiOBr}/\text{Bi}_2\text{WO}_6$  (8:1) delivered the highest degradation efficiency for removing Rh B, TC, CIP, and MB (100%, 96%, 90% and 94%). Ren et al. [78] synthesized  $\text{Bi}_2\text{WO}_6/\text{BiOBr}$  composites via a one-step solvothermal route by using [C16mim] Br ionic liquid as the Br source. In this composite,  $\text{Bi}_2\text{WO}_6$  nanoparticles wrapped on flower-like  $\text{BiOBr}$  and formed a type II heterojunction, which promoted the transfer and separation of charge carriers and enhanced visible light harvesting. The optimized composite with a W/Br ratio of 1:2 delivered the highest photocatalytic activity for the degradation of MB, Rh B, and TC. Chen et al. [79] synthesized a  $\text{BiOBr}/\text{Bi}/\text{Bi}_2\text{WO}_6$  composite via the hydrothermal method to construct a Z-scheme heterojunction for enhancing photocatalytic activity. Due to the synergistic effect of the Z-scheme  $\text{BiOBr}/\text{Bi}_2\text{WO}_6$  heterojunction and

the surface plasmon resonance (SPR) effect of Bi, the optimized 20%BiOBr/7%Bi/Bi<sub>2</sub>WO<sub>6</sub> achieved the fast degradation of Rh B under visible light, and the degradation rate of Rh B reached 98.02% within 60 min. He et al. [80] prepared a hydrangea-like BiOBr/Bi<sub>2</sub>WO<sub>6</sub> composite via an ionic liquid-assisted hydrothermal route. The core-shell structured 3D/2D BiOBr/Bi<sub>2</sub>WO<sub>6</sub> (Figure 7a) displayed an enhanced degradation performance for removing organic dye and drugs due to the formation of the Z-scheme heterojunction.

Besides BiOCl and BiOBr, flower-like BiOI/Bi<sub>2</sub>WO<sub>6</sub> microspheres were prepared via the hydrothermal route for the degradation of phenol [81]. The formed heterojunction between Bi<sub>2</sub>WO<sub>6</sub> and BiOI enhanced the separation efficiency of the electron and hole, further improving the photocatalytic activity. To further improve the photoactivity of the Bi<sub>2</sub>WO<sub>6</sub>/BiOI composite, Zheng et al. [82] deposited Ag nanoparticles onto the surface of Bi<sub>2</sub>WO<sub>6</sub>/BiOI to fabricate a Bi<sub>2</sub>WO<sub>6</sub>/BiOI/Ag heterojunction (Figure 7b). Besides the function of the heterojunction structure, Ag particles contributed to the SPR effect, which extended the visible-light absorption and accelerated the separation/transfer of photogenerated carriers. The sample of Bi<sub>2</sub>WO<sub>6</sub>/BiOI/Ag-8 displayed the highest activity for the degradation of tetracycline and a superior recycling performance.

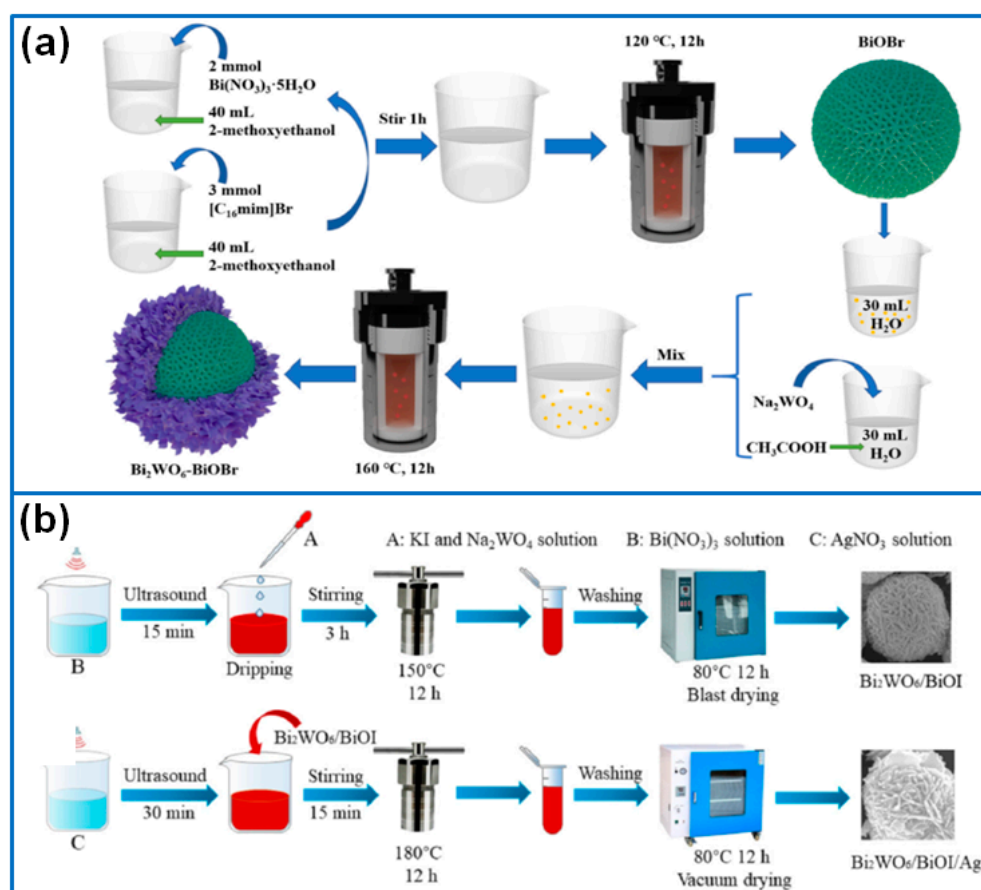


**Figure 7.** Fabrication process of (a) 3D/2D BiOBr/Bi<sub>2</sub>WO<sub>6</sub> [80]. Copyright (2021) Elsevier. (b) Bi<sub>2</sub>WO<sub>6</sub>/BiOI/Ag heterojunction [82]. Copyright (2022) Elsevier.

Qiang et al. [83] synthesized I-doped Bi<sub>2</sub>O<sub>2</sub>CO<sub>3</sub>/Bi<sub>2</sub>WO<sub>6</sub> heterojunction microspheres via the ionic liquid-assisted solvothermal method. The I-doped heterojunction adjusted the energy band structure and enhanced visible light adsorption, charge separation, and proton reduction. Therefore, the doped composite presented outstanding photocatalytic performance for the degradation of TC and Rh B. Wu et al. [84] prepared 3D flower-like BiPO<sub>4</sub>/Bi<sub>2</sub>WO<sub>6</sub> composites via the hydrothermal method for the degradation of Rh B under visible light irradiation. The hybridization of two components accelerated the separation efficiency of charge carriers and inhibited their recombination. The composite containing

15% BiPO<sub>4</sub> displayed the highest photocatalytic activity, which degraded 92% Rh B within 100 min, about 3.7 and 1.4 times higher than that of BiPO<sub>4</sub> and Bi<sub>2</sub>WO<sub>6</sub>, respectively. Zhang et al. [85] deposited Bi<sub>2</sub>Sn<sub>2</sub>O<sub>7</sub> (BSO) nanoparticles onto Bi<sub>2</sub>WO<sub>6</sub> (BWO) nanosheets to fabricate flower-like Bi<sub>2</sub>Sn<sub>2</sub>O<sub>7</sub>/Bi<sub>2</sub>WO<sub>6</sub> hierarchical composite photocatalysts. When used for the degradation of Rh B under visible light, the 7% BSO/BWO composite displayed the best photocatalytic activity, much better than that of pure BWO or BSO, due to the promoted separation of the photogenerated electron-hole pairs.

Tao et al. [86] synthesized Bi<sub>2</sub>WO<sub>6</sub> nanosheets (NSs) on electrospun BiFeO<sub>3</sub> nanofibers (NFs) to fabricate 1D discrete heterojunction nanofibers. The ferromagnetic feature of BiFeO<sub>3</sub> facilitated the recycling treatment, and the high surface area facilitated the photocatalytic reaction by providing abundant active sites. Moreover, the 1D heterojunction promoted the separation/transport of photogenerated charges. As a result, the reaction rate constant of the nanofiber-like photocatalyst for Rh B degradation was 36.7 times and 8.7 times higher than that of pure BiFeO<sub>3</sub> and Bi<sub>2</sub>WO<sub>6</sub>, respectively. Integrating the solvothermal reaction with the electrospinning technique, Teng et al. [87] prepared a one-dimensional CuBi<sub>2</sub>O<sub>4</sub>/Bi<sub>2</sub>WO<sub>6</sub> fiber composite. Due to the formation of a Z-type heterojunction, a fiber-like photocatalyst achieved the fast degradation of more than 90% TCH within 120 min. In addition, Wang et al. [88] created flower-flake-like CuBi<sub>2</sub>O<sub>4</sub>/BWO composite via a hydrothermal route. Under the irradiation of visible light, the composite containing 60 wt% CuBi<sub>2</sub>O<sub>4</sub> delivered the highest photocatalytic activity, which degraded 93% TC (20 mg/L) within 1 h. The superior performance was ascribed to the improved visible light absorption, interfacial charge transfer and separation, and the prolonged lifetime of photogenerated carriers.

### 3.6. Bi<sub>2</sub>WO<sub>6</sub>/Metal Tungstates Composite

Metal tungstates (MWO<sub>4</sub>) show the wolframite-type monoclinic structure and scheelite-type tetragonal structure, which received more attention in the photocatalytic field. The combination of Bi<sub>2</sub>WO<sub>6</sub> with metal tungstates integrates the advantage of each component and presents enhanced photocatalytic activity for the degradation of organic pollutants. In this field, Kumar et al. [89] synthesized a Bi<sub>2</sub>WO<sub>6</sub>/ZnWO<sub>4</sub> composite photocatalyst via the modified hydrothermal method. The bi-crystalline framework of Bi<sub>2</sub>WO<sub>6</sub> and ZnWO<sub>4</sub> played a synergistic effect, which reduced the crystallite size and band gap and effectively separated and transferred the photo-generated electron-hole pairs. Under UV irradiation, the optimized 30% Bi<sub>2</sub>WO<sub>6</sub>/ZnWO<sub>4</sub> delivered the maximum degradation performance for the removal of Plasmocorinth B dye. Miao et al. [90] prepared Sb<sub>2</sub>WO<sub>6</sub>/Bi<sub>2</sub>WO<sub>6</sub> composite photocatalysts and evaluated their photocatalytic activity for the degradation of Rh B and MO. The composite showed an increased specific surface area and an enhanced visible-light absorption capability, and it suppressed the recombination of electron-hole pairs. The composite containing 6% Sb achieved the fast degradation of 100% Rh B and 70% MO within 90 min, much better than pure single phase Bi<sub>2</sub>WO<sub>6</sub> and Sb<sub>2</sub>WO<sub>6</sub>. Ni et al. [91] synthesized a flower-like Ag<sub>2</sub>WO<sub>4</sub>/Bi<sub>2</sub>WO<sub>6</sub> (AWO/BWO) composite for the degradation of Rh B. AWO and BWO formed a direct Z-scheme heterojunction, which promoted the migration of interface charges, enhanced the light absorption capability, and inhibited the recombination of the electron-hole pairs. The composite containing 3 wt% AWO exhibited the highest activity, which degraded nearly 100% Rh B within 150 min, 11.5-fold and 1.5-fold higher than that of pristine AWO and BWO.

## 4. Bi<sub>2</sub>WO<sub>6</sub>-Based Ternary Composite

Besides Bi<sub>2</sub>WO<sub>6</sub>-based binary heterojunction composites, lots of Bi<sub>2</sub>WO<sub>6</sub>-containing ternary composites were developed as high-performance photocatalysts. From the reported Bi<sub>2</sub>WO<sub>6</sub>-based ternary composites, commonly used components involve carbon materials, g-C<sub>3</sub>N<sub>4</sub>, BiOX, AgBr, Ag<sub>2</sub>CO<sub>3</sub>, Ag<sub>2</sub>O, Cu<sub>2</sub>O, TiO<sub>2</sub>, ZnO, Ti<sub>3</sub>C<sub>2</sub>, Bi<sub>2</sub>MoO<sub>6</sub>, BiPO<sub>4</sub>, and Au/Ag nanoparticles. Compared to binary composites, the advantage of ternary composites exhibits optimized light harvesting capability and photocatalytic activity due

to the constructed double heterostructure interfaces and the synergistic effect derived from three components. In view of the broad selectivity of semiconductor candidates, it is hard to summarize the design principle of  $\text{Bi}_2\text{WO}_6$ -based ternary composites. However, the fixed binary combination of  $\text{Bi}_2\text{WO}_6/\text{g-C}_3\text{N}_4$ ,  $\text{Bi}_2\text{WO}_6/\text{carbon materials}$ ,  $\text{Bi}_2\text{WO}_6/\text{Au}$  or  $\text{Ag}$ -based materials, and  $\text{Bi}_2\text{WO}_6/\text{Bi-series semiconductors}$  is reported to hybridize with the third component.

#### 4.1. The Composite of $\text{Bi}_2\text{WO}_6/\text{g-C}_3\text{N}_4/\text{Other Materials}$

In respect of the  $\text{Bi}_2\text{WO}_6/\text{g-C}_3\text{N}_4$  combination, Zhang et al. [92] prepared a dual Z-scheme  $\text{BiSI}/\text{Bi}_2\text{WO}_6/\text{g-C}_3\text{N}_4$  photocatalyst via hydrothermal method. The generation of dual Z-scheme heterojunction promoted the transfer and separation of photogenerated electron–hole pairs. When used for the degradation of TC, Rh B, and chlortetracycline (CTC), the optimized  $\text{BiSI}/\text{Bi}_2\text{WO}_6/20\%\text{g-C}_3\text{N}_4$  exhibited the highest photocatalytic activity, much better than that of the single and binary systems. Sun et al. [93] fabricated a double Z-scheme  $\text{g-C}_3\text{N}_4/\text{Bi}_2\text{MoO}_6/\text{Bi}_2\text{WO}_6$  (CN/MO/WO) composite for the degradation of TC. In this ternary system,  $\text{g-C}_3\text{N}_4$  enhanced the specific surface area and accelerated the carrier transfer.  $\text{Bi}_2\text{WO}_6$  and  $\text{Bi}_2\text{MoO}_6$  extended the light absorption range and inhibited the recombination of photogenerated electron–hole pairs. As a result, the optimized 15% CN/MO/WO composite achieved the fast photodegradation of 98% TC within 30 min under the irradiation of visible light. Zhou et al. [94] synthesized dual Z-scheme  $\text{BiOBr}/\text{g-C}_3\text{N}_4/\text{Bi}_2\text{WO}_6$  photocatalysts via one-pot hydrothermal reaction. The dual heterojunction effectively suppressed the recombination of photogenerated carriers and presented superior photocatalytic activity, which degraded 90% TC within 40 min under the irradiation of visible light. In addition, a  $\text{Bi}_2\text{WO}_6/\text{BiOI}/\text{g-C}_3\text{N}_4$  ternary composite photocatalyst was prepared for the degradation of TC [95], and the optimized composite degraded over 90% TC within 120 min. Moreover, the ternary photocatalyst also exhibited a superior performance for the degradation of municipal waste transfer station leachate.

Hu et al. [96] fabricated a ternary heterojunction  $\text{g-C}_3\text{N}_4/\text{BiVO}_4\text{-Bi}_2\text{WO}_6$  photocatalyst by the intercalation of a  $\text{BiVO}_4\text{-Bi}_2\text{WO}_6$  composite into compressed layered  $\text{g-C}_3\text{N}_4$  nanosheets. The compressed layer structure accelerated the transfer of electrons and the generation of superoxide radicals, which enhanced photocatalytic activity, and the degradation efficiency of Rh B and TC was 96.7% and 94.8% within 60 min, respectively. In another work, a 2D/2D/2D  $\text{Bi}_2\text{WO}_6/\text{g-C}_3\text{N}_4/\text{Ti}_3\text{C}_2$  composite (Figure 8a) was prepared via a one-step hydrothermal reaction [97]. In this system, seamless interfacial contact of the 2D heterojunction facilitated the separation and transfer of photogenerated electron–hole pairs. Moreover,  $\text{Ti}_3\text{C}_2$  also promoted charge separation. As a result, the composite achieved the fast photodegradation of CIP, and the reaction rate constant was 4.78 times higher than that of  $\text{Bi}_2\text{WO}_6$ . Li et al. [98] prepared a 2D/2D Z-scheme  $\text{g-C}_3\text{N}_4/\text{Au}/\text{Bi}_2\text{WO}_6$  (CN/Au/BWO) composite for the photodegradation of Rh B. Serving as a redox mediator, Au nanoparticles accelerated the transmission and separation of photogenerated carriers. Moreover, the 2D/2D Z-scheme structure provided abundant active sites for enhancing the photocatalytic activity. The CN/Au(1)/BWO sample degraded 88.7% Rh B within 30 min, and the rate constant was 1.48-fold and 1.62-fold higher than that of pure BWO and CN, respectively. To further enhance the photocatalytic activity of the  $\text{g-C}_3\text{N}_4/\text{Bi}_2\text{WO}_6$  Z-scheme heterojunction, Jia et al. [99] introduced nitrogen-doped carbon quantum dots (NCQs) onto a  $\text{g-C}_3\text{N}_4/\text{Bi}_2\text{WO}_6$  interface to form  $\text{g-C}_3\text{N}_4/\text{Bi}_2\text{WO}_6/\text{NCQs}$  ternary composites (Figure 8b). The NCQs extended the light absorption range and promoted the transfer and separation of photogenerated electron–hole pairs. Compared to single or binary composites, the ternary composite showed the highest degradation efficiency for the removal of Rh B and TC under visible light irradiation.



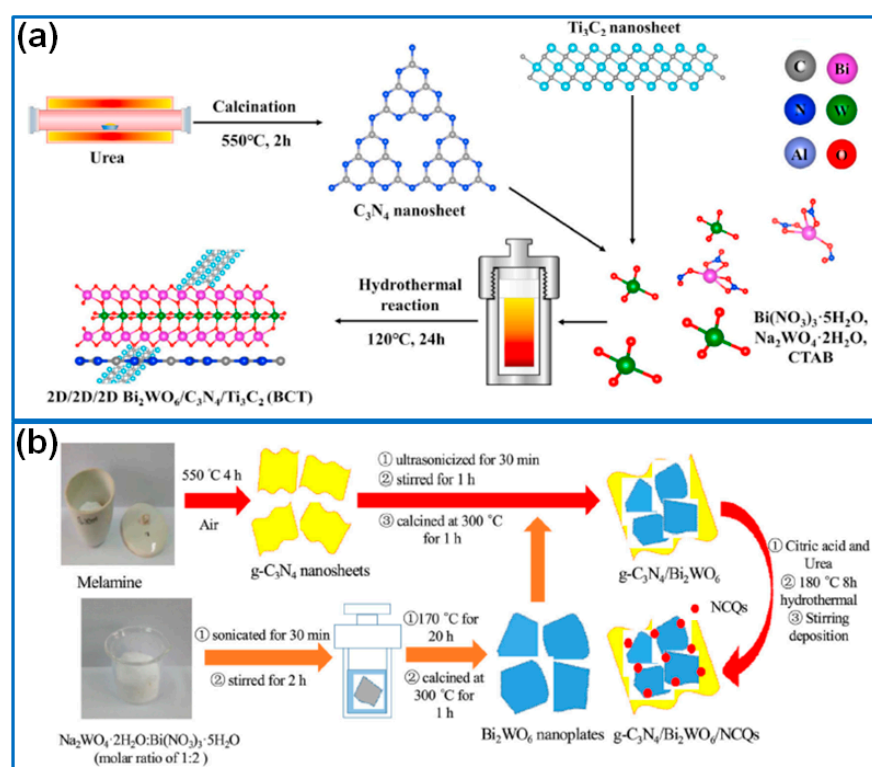


**Figure 8.** Preparation of (a)  $\text{Bi}_2\text{WO}_6/\text{g-C}_3\text{N}_4/\text{Ti}_3\text{C}_2$  [97]. Copyright (2020) Elsevier. (b)  $\text{g-C}_3\text{N}_4/\text{Bi}_2\text{WO}_6/\text{NCQs}$  ternary composite [99]. Copyright (2020) Elsevier.

#### 4.2. The Composite of $\text{Bi}_2\text{WO}_6$ /Carbon/Other Materials

In the field of  $\text{Bi}_2\text{WO}_6$ /carbon materials, Guan et al. [100] synthesized a ternary  $\text{AgBr}/\text{GO}/\text{Bi}_2\text{WO}_6$  Z-scheme photocatalyst and discussed the effect of  $\text{AgBr}$  and  $\text{GO}$  fractions on photocatalytic activity. The optimized  $15\%\text{AgBr}/5\%\text{GO}/\text{Bi}_2\text{WO}_6$  delivered the highest degradation efficiency for the removal of 84% TC under visible light, and the reaction kinetic constant was about 3.16-fold and 4.60-fold higher than that of pure  $\text{Bi}_2\text{WO}_6$  and  $\text{AgBr}$ , respectively. The superior performance was due to an extended visible light adsorption range and an enhanced charge separation and transfer. Zhu et al. [101] prepared a  $\text{GO}@\text{BiOI}/\text{Bi}_2\text{WO}_6$  composite for the removal of Bisphenol A (BPA). In this ternary system,  $\text{GO}$  effectively modified the surface of  $\text{BiOI}/\text{Bi}_2\text{WO}_6$  and improved the physico-chemical property. The optimized composite degraded 81% BPA within 5 h under the irradiation of UV-vis light. Tian et al. [102] prepared a Z-scheme flower-like  $\text{Bi}_2\text{MoO}_6/\text{Bi}_2\text{WO}_6/\text{MWCNTs}$  photocatalyst via hydrothermal route. Under visible light irradiation, the ternary composite degraded 96% reactive blue 19 (RB-19) within 4 h, the photocatalytic efficiency was much higher than that of  $\text{Bi}_2\text{MoO}_6/\text{MWCNTs}$ , and pure  $\text{Bi}_2\text{MoO}_6$  and  $\text{Bi}_2\text{WO}_6$ . Niu et al. [103] synthesized  $\text{Bi}_2\text{WO}_6/\text{C}@\text{Cu}_2\text{O}$  Z-scheme photocatalysts for TC degradation. The wrapped carbon layer on  $\text{Cu}_2\text{O}$  avoided the photo-corrosion of  $\text{Cu}_2\text{O}$ . Furthermore, the oxygen-containing groups in the carbon layer decreased interfacial resistance and promoted electron transfer. The degradation rate constant of the ternary composite was 2.8 times higher than that of pure  $\text{Bi}_2\text{WO}_6$ .

#### 4.3. The Composite of $\text{Bi}_2\text{WO}_6$ /Au or Ag-Based Materials/Other Materials

Among the  $\text{Bi}_2\text{WO}_6$ /Ag-based materials, Wang et al. [104] prepared a  $\text{Ag}_2\text{CO}_3/\text{AgBr}/\text{Bi}_2\text{WO}_6$  ternary photocatalyst via a precipitation method. When used for the degradation of Rh B, the degradation rate of the ternary composite was 95.1% within 60 min under solar illumination, and the degradation efficiency was much higher than that of each component. Gang et al. [105] synthesized a  $\text{Ag}/\text{AgBr}/\text{Bi}_2\text{WO}_6$  composite via the oil/water self-assembly method. In this ternary composite,  $\text{Ag}/\text{AgBr}$  was uniformly dispersed on

the  $\text{Bi}_2\text{WO}_6$  surface, which extended the visible-light absorption range for the surface plasmonic resonance (SPR) effect of Ag. Moreover, the composite accelerated the separation of photogenerated charges. When utilized for the degradation of Rh B and phenol, the ternary composite presented optimum photocatalytic activity under visible light, much better than Ag/AgBr and pure  $\text{Bi}_2\text{WO}_6$ . Jin et al. [106] prepared a  $\text{Au@TiO}_2/\text{Bi}_2\text{WO}_6$  composite via a sol-gel method followed by hydrothermal reaction. In this ternary system, core-shell structured  $\text{Au@TiO}_2$  nanoparticles were dispersed on flower-like  $\text{Bi}_2\text{WO}_6$  nanosheets. The formation of a Z-scheme heterojunction and SPR effect of Au promoted the generation, separation, and interfacial transfer of photogenerated charge carriers. When served for the degradation of sulfamethoxazole (SMX) and TCH under visible light, the degradation rate was 96.9% and 95.0% within 75 min, respectively. Moreover, the degradation rate constant was 7.2 times and 1.9 times higher than that of pure  $\text{Bi}_2\text{WO}_6$ , respectively.

#### 4.4. The Composite of $\text{Bi}_2\text{WO}_6/\text{Bi}$ -Series Semiconductors/Other Materials

In the field of  $\text{Bi}_2\text{WO}_6/\text{Bi}$ -series semiconductors, Zhu et al. [107] prepared a magnetic  $\text{Bi}_2\text{WO}_6/\text{BiOI@Fe}_3\text{O}_4$  ternary composite for the photodegradation of TC. The optimized  $\text{Bi}_2\text{WO}_6/\text{BiOI@5\%Fe}_3\text{O}_4$  sample showed the highest TC degradation rate of 97%, much higher than that of pure  $\text{Bi}_2\text{WO}_6$  (63%). Moreover, the spent powder can be magnetically recycled, and the recycled sample also exhibited good photocatalytic activity. Combining the electrostatic spinning technique, Chen et al. [108] fabricated 1D magnetic flower-like  $\text{CoFe}_2\text{O}_4@\text{Bi}_2\text{WO}_6@\text{BiOBr}$  photocatalysts for the degradation of Rh B. The resulting flower-like heterojunction enhanced the specific surface area and accelerated the separation of photogenerated charge carriers. Consequently, the ternary composite degraded 92.08% Rh B within 3 h.

#### 4.5. Other Composites

In view of the high surface area and tight interfacial contact of 2D nanomaterials [109–111], Sharma et al. [112] prepared a 2D-2D-2D  $\text{ZnO}/\text{Bi}_2\text{WO}_6/\text{Ti}_3\text{C}_2$  ternary composite photocatalyst via two-step electrostatic assembly. The optimized ZBT05 containing 5 wt%  $\text{Ti}_3\text{C}_2$  delivered the highest degradation rate (~77%) for the removal of ciprofloxacin (CFX) within 160 min due to the enhanced photogenerated charge carrier separation caused by the generated ternary interface. Besides ternary composites, the composite photocatalysts composed of four or five components were reported for enhancing photocatalytic activity. In this respect, Ma et al. [113] prepared a GO-modified  $\text{Ag}/\text{Ag}_2\text{O}/\text{BiPO}_4/\text{Bi}_2\text{WO}_6$  multi-component composite photocatalyst and investigated the photocatalytic activity for the degradation of Rh B and amoxicillin (AMX). The composite exhibited a small size, fast charge transfer efficiency, and extended light absorption range, which presented enhanced photocatalytic activity for the degradation of AMX, Rh B, and E. coli under visible light irradiation.

## 5. Conclusions and Prospects

To sum up, the advances of  $\text{Bi}_2\text{WO}_6$ -based photocatalysts are summarized in this review, including morphology control, the surface modification and heteroatom doping of  $\text{Bi}_2\text{WO}_6$ ,  $\text{Bi}_2\text{WO}_6$ -based binary composites, and  $\text{Bi}_2\text{WO}_6$ -based ternary composites. The most popular synthesis method of  $\text{Bi}_2\text{WO}_6$  is the hydrothermal or solvothermal method, and the reaction temperature and time heavily affect the microstructure and photocatalytic performance of  $\text{Bi}_2\text{WO}_6$ . The surfactants of CTAB and PVP were used to adjust the microstructure of  $\text{Bi}_2\text{WO}_6$ . Furthermore, Au-decorated  $\text{Bi}_2\text{WO}_6$  hollow microspheres were synthesized to utilize the SPR effect of Au nanoparticles. Heteroatom doping can be used to enhance the photoactivity of  $\text{Bi}_2\text{WO}_6$ . Among various dopants, N, F, Cl, and I serve as non-metal dopants for doping  $\text{Bi}_2\text{WO}_6$ . In addition, Fe, Ti, Sr, Er, La, Au, Ag, and Mo are used to fabricate metal-doped  $\text{Bi}_2\text{WO}_6$ . Besides single atom doping, (La, Mo) co-doped  $\text{Bi}_2\text{WO}_6$  was reported to enhance the photoactivity of  $\text{Bi}_2\text{WO}_6$  by adjusting the particle size and lattice spacing. In view of the limited photocatalytic activity of single  $\text{Bi}_2\text{WO}_6$ , the

development of  $\text{Bi}_2\text{WO}_6$ -based binary and ternary composites has become a major topic for constructing high-performance photocatalysts.  $\text{Bi}_2\text{WO}_6$ -based binary composites show a wide research range for the diversity of alternative materials. The existing  $\text{Bi}_2\text{WO}_6$ -based binary composites can be classified into six types:  $\text{Bi}_2\text{WO}_6$ /carbon or MOF composite,  $\text{Bi}_2\text{WO}_6$ / $g\text{-C}_3\text{N}_4$  composite,  $\text{Bi}_2\text{WO}_6$ /metal oxides composite,  $\text{Bi}_2\text{WO}_6$ /metal sulfides composite,  $\text{Bi}_2\text{WO}_6$ /Bi-series composite, and  $\text{Bi}_2\text{WO}_6$ /metal tungstates composite. Due to the diversity of target organic pollutants, and the difference of pollutant concentration, light source or powder, and catalyst dosage, it is very difficult to compare the photocatalytic activity of different  $\text{Bi}_2\text{WO}_6$ -based binary composites. Compared to other semiconductors,  $g\text{-C}_3\text{N}_4$  and metal oxides are widely used to hybridize with  $\text{Bi}_2\text{WO}_6$ , and the resulting  $\text{Bi}_2\text{WO}_6$ / $g\text{-C}_3\text{N}_4$  and  $\text{Bi}_2\text{WO}_6$ /metal oxides composites deliver enhanced photodegradation efficiency, which is much better than each component. Besides  $\text{Bi}_2\text{WO}_6$ -based binary composites, lots of  $\text{Bi}_2\text{WO}_6$ -based ternary composites were developed as high-performance photocatalysts. The commonly used components include carbon materials,  $g\text{-C}_3\text{N}_4$ , BiOX, AgBr,  $\text{Ag}_2\text{CO}_3$ ,  $\text{Ag}_2\text{O}$ ,  $\text{Cu}_2\text{O}$ ,  $\text{TiO}_2$ , ZnO,  $\text{Ti}_3\text{C}_2$ ,  $\text{Bi}_2\text{MoO}_6$ ,  $\text{BiPO}_4$ , and Au/Ag nanoparticles. According to the material type, binary  $\text{Bi}_2\text{WO}_6$ / $g\text{-C}_3\text{N}_4$ ,  $\text{Bi}_2\text{WO}_6$ /carbon materials,  $\text{Bi}_2\text{WO}_6$ /Au or Ag-based materials, and  $\text{Bi}_2\text{WO}_6$ /Bi-series semiconductors were fabricated for further hybridizing with the third component, and they present outstanding photocatalytic activity for the formation of double heterostructures and the synergistic effect of three components. In addition, a GO modified Ag/Ag<sub>2</sub>O/BiPO<sub>4</sub>/ $\text{Bi}_2\text{WO}_6$  multi-component composite was synthesized to further improve photocatalytic activity.

Based on the summary above, abundant progress has been achieved in  $\text{Bi}_2\text{WO}_6$ -based photocatalysts. However, some urgent problems still exist, such as the controllable microstructure, the suitable component and ratio optimization, and the photocatalytic mechanism of different  $\text{Bi}_2\text{WO}_6$ -based composites. Aiming to solving the three problems mentioned above, we put forward the following promising research trends:

- (1) The controllable synthesis and microstructure optimization of  $\text{Bi}_2\text{WO}_6$  and  $\text{Bi}_2\text{WO}_6$ -based composite. The ideal microstructures of photocatalysts include hierarchical hollow structures, flowers, or spheres with a high specific surface area. Moreover, binary or ternary composites should have a strong interfacial binding strength, and the ratio optimization of different components is a major task.
- (2) The selection of suitable candidate semiconductor photocatalysts. The selection of semiconductors should consider the band gap feature of  $\text{Bi}_2\text{WO}_6$ , and the resulting  $\text{Bi}_2\text{WO}_6$ -based composite should form a Z-scheme, S-scheme heterojunction, or double heterojunctions. In addition, the heteroatom doping and introduction of noble metal nanoparticles can be adopted as an effective strategy for enhancing photocatalytic activity.
- (3) The combination of theoretical calculation and experimental results clarify the photocatalytic mechanism. The photocatalytic mechanism of the  $\text{Bi}_2\text{WO}_6$ -based composite is the difficulty for designing high-performance hybrid photocatalysts. Besides the traditional characterization techniques, theory computations should be paid more attention for clarifying the photocatalytic mechanism.

**Author Contributions:** Conceptualization, H.J. and X.H.; validation, J.H., C.D. and B.L.; writing—original draft preparation, H.J.; writing—review and editing, X.H. and B.L. All authors have read and agreed to the published version of the manuscript.

**Funding:** This work was funded by Guangdong Provincial Key Laboratory of Battery Recycling and Reuse (2021B1212050002) and the Innovation Team of Universities of Guangdong Province (2022KCXTD030).

**Institutional Review Board Statement:** Not applicable.

**Informed Consent Statement:** Not applicable.

**Conflicts of Interest:** The authors declare no conflict of interest.

## References

1. Chen, T.; Liu, L.; Hu, C.; Huang, H. Recent advances on Bi<sub>2</sub>WO<sub>6</sub>-based photocatalysts for environmental and energy applications. *Chin. J. Catal.* **2021**, *42*, 1413–1438. [[CrossRef](#)]
2. Orimolade, B.O.; Idris, A.O.; Feleni, U.; Mamba, B. Recent advances in degradation of pharmaceuticals using Bi<sub>2</sub>WO<sub>6</sub> mediated photocatalysis—A comprehensive review. *Environ. Pollut.* **2021**, *289*, 117891. [[CrossRef](#)] [[PubMed](#)]
3. Duan, Z.; Zhu, Y.; Hu, Z.; Zhang, J.; Liu, D.; Luo, X.; Gao, M.; Lei, L.; Wang, X.; Zhao, G. Micro-patterned NiFe<sub>2</sub>O<sub>4</sub>/Fe-TiO<sub>2</sub> composite films: Fabrication, hydrophilicity and application in visible-light-driven photocatalysis. *Ceram. Int.* **2020**, *46*, 27080–27091. [[CrossRef](#)]
4. Chen, J.; Chen, X.; Li, N.; Liang, Y.; Yu, C.; Yao, L.; Lai, Y.; Huang, Y.; Chen, H.; Chen, Y.; et al. Enhanced photocatalytic activity of La<sub>1-x</sub>Sr<sub>x</sub>CoO<sub>3</sub>/Ag<sub>3</sub>PO<sub>4</sub> induced by the synergistic effect of doping and heterojunction. *Ceram. Int.* **2021**, *47*, 19923–19933. [[CrossRef](#)]
5. Xiong, J.; Li, W.; Zhao, K.; Li, W.; Cheng, G. Engineered zinc oxide nanoaggregates for photocatalytic removal of ciprofloxacin with structure dependence. *J. Nanopart. Res.* **2020**, *22*, 155. [[CrossRef](#)]
6. Wang, H.; Sun, T.; Xu, N.; Zhou, Q.; Chang, L. 2D sodium titanate nanosheet encapsulated Ag<sub>2</sub>O-TiO<sub>2</sub> p-n heterojunction photocatalyst: Improving photocatalytic activity by the enhanced adsorption capacity. *Ceram. Int.* **2021**, *47*, 4905–4913. [[CrossRef](#)]
7. Hong, X.; Li, Y.; Wang, X.; Long, J.; Liang, B. Carbon nanosheet/MnO<sub>2</sub>/BiOCl ternary composite for degradation of organic pollutants. *J. Alloy. Compd.* **2022**, *891*, 162090. [[CrossRef](#)]
8. Khedr, T.M.; Wang, K.; Kowalski, D.; El-Sheikh, S.M.; Abdeldayem, H.M.; Ohtani, B.; Kowalska, E. Bi<sub>2</sub>WO<sub>6</sub>-based Z-scheme photocatalysts: Principles, mechanisms and photocatalytic applications. *J. Environ. Chem. Eng.* **2022**, *10*, 107838. [[CrossRef](#)]
9. Lai, M.T.L.; Lai, C.W.; Lee, K.M.; Chook, S.W.; Yang, T.C.K.; Chong, S.H.; Juan, J.C. Facile one-pot solvothermal method to synthesize solar active Bi<sub>2</sub>WO<sub>6</sub> for photocatalytic degradation of organic dye. *J. Alloy. Compd.* **2019**, *801*, 502–510. [[CrossRef](#)]
10. Helen Selvi, M.; Reddy Vanga, P.; Ashok, A. Photocatalytic application of Bi<sub>2</sub>WO<sub>6</sub> nanoplates structure for effective degradation of methylene blue. *Optik* **2018**, *173*, 227–234. [[CrossRef](#)]
11. Guo, X.; Wu, D.; Long, X.; Zhang, Z.; Wang, F.; Ai, G.; Liu, X. Nanosheets-assembled Bi<sub>2</sub>WO<sub>6</sub> microspheres with efficient visible-light-driven photocatalytic activities. *Mater. Charact.* **2020**, *163*, 110297. [[CrossRef](#)]
12. Bai, J.; Zhang, B.; Xiong, T.; Jiang, D.; Ren, X.; Lu, P.; Fu, M. Enhanced visible light driven photocatalytic performance of Bi<sub>2</sub>WO<sub>6</sub> nano-catalysts by introducing oxygen vacancy. *J. Alloy. Compd.* **2021**, *887*, 161297. [[CrossRef](#)]
13. Chankhanittha, T.; Somaudon, V.; Photiwat, T.; Hemavibool, K.; Nanan, S. Preparation, characterization, and photocatalytic study of solvothermally grown CTAB-capped Bi<sub>2</sub>WO<sub>6</sub> photocatalyst toward photodegradation of Rhodamine B dye. *Opt. Mater.* **2021**, *117*, 111183. [[CrossRef](#)]
14. Zhou, Y.; Lv, P.; Zhang, W.; Meng, X.; He, H.; Zeng, X.; Shen, X. Pristine Bi<sub>2</sub>WO<sub>6</sub> and hybrid Au-Bi<sub>2</sub>WO<sub>6</sub> hollow microspheres with excellent photocatalytic activities. *Appl. Surf. Sci.* **2018**, *457*, 925–932. [[CrossRef](#)]
15. Hoang, L.H.; Phu, N.D.; Peng, H.; Chen, X.B. High photocatalytic activity N-doped Bi<sub>2</sub>WO<sub>6</sub> nanoparticles using a two-step microwave-assisted and hydrothermal synthesis. *J. Alloy. Compd.* **2018**, *744*, 228–233. [[CrossRef](#)]
16. Chen, Y.; Zhang, F.; Guan, S.; Shi, W.; Wang, X.; Huang, C.; Chen, Q. Visible light degradation of tetracycline by hierarchical nanoflower structured fluorine-doped Bi<sub>2</sub>WO<sub>6</sub>. *Mater. Sci. Semicon. Proc.* **2022**, *140*, 106385. [[CrossRef](#)]
17. Phuruangrat, A.; Dumrongrojthanath, P.; Thongtem, S.; Thongtem, T. Hydrothermal synthesis of I-doped Bi<sub>2</sub>WO<sub>6</sub> for using as a visible-light-driven photocatalyst. *Mater. Lett.* **2018**, *224*, 67–70. [[CrossRef](#)]
18. Hu, T.; Li, H.; Du, N.; Hou, W. Iron-Doped Bismuth Tungstate with an Excellent Photocatalytic Performance. *ChemCatChem* **2018**, *10*, 3040–3048. [[CrossRef](#)]
19. Arif, M.; Zhang, M.; Yao, J.; Yin, H.; Li, P.; Hussain, I.; Liu, X. Layer-assembled 3D Bi<sub>2</sub>WO<sub>6</sub> hierarchical architectures by Ti-doping for enhanced visible-light driven photocatalytic and photoelectrochemical performance. *J. Alloy. Compd.* **2019**, *792*, 878–893. [[CrossRef](#)]
20. Maniyazagan, M.; Hussain, M.; Kang, W.S.; Kim, S.J. Hierarchical Sr-Bi<sub>2</sub>WO<sub>6</sub> photocatalyst for the degradation of 4-nitrophenol and methylene blue. *J. Ind. Eng. Chem.* **2022**, *110*, 168–177. [[CrossRef](#)]
21. Qiu, Y.; Lu, J.; Yan, Y.; Niu, J. Enhanced visible-light-driven photocatalytic degradation of tetracycline by 16% Er<sup>3+</sup>-Bi<sub>2</sub>WO<sub>6</sub> photocatalyst. *J. Hazard. Mater.* **2022**, *422*, 126920. [[CrossRef](#)] [[PubMed](#)]
22. Ning, J.; Zhang, J.; Dai, R.; Wu, Q.; Zhang, L.; Zhang, W.; Yan, J.; Zhang, F. Experiment and DFT study on the photocatalytic properties of La-doped Bi<sub>2</sub>WO<sub>6</sub> nanoplate-like materials. *Appl. Surf. Sci.* **2022**, *579*, 152219. [[CrossRef](#)]
23. Phuruangrat, A.; Buapoon, S.; Bunluesak, T.; Suebsom, P.; Wannapop, S.; Thongtem, T.; Thongtem, S. Hydrothermal preparation of Au-doped Bi<sub>2</sub>WO<sub>6</sub> nanoplates for enhanced visible-light-driven photocatalytic degradation of rhodamine B. *Solid State Sci.* **2022**, *128*, 106881. [[CrossRef](#)]
24. Phu, N.D.; Hoang, L.H.; Van Hai, P.; Huy, T.Q.; Chen, X.B.; Chou, W.C. Photocatalytic activity enhancement of Bi<sub>2</sub>WO<sub>6</sub> nanoparticles by Ag doping and Ag nanoparticles modification. *J. Alloy. Compd.* **2020**, *824*, 153914. [[CrossRef](#)]
25. Longchin, P.; Sakulsermsuk, S.; Wetchakun, K.; Wetchakun, N. Synergistic effect of La and Mo co-doping on the enhanced photocatalytic activity of Bi<sub>2</sub>WO<sub>6</sub>. *Mater. Lett.* **2021**, *305*, 130779. [[CrossRef](#)]
26. Zhao, Y.; Liang, X.; Hu, X.; Fan, J. rGO/Bi<sub>2</sub>WO<sub>6</sub> composite as a highly efficient and stable visible-light photocatalyst for norfloxacin degradation in aqueous environment. *J. Colloid Interface Sci.* **2021**, *589*, 336–346. [[CrossRef](#)] [[PubMed](#)]

27. Arya, M.; Kaur, M.; Kaur, A.; Singh, S.; Devi, P.; Kansal, S.K. Hydrothermal synthesis of rGO-Bi<sub>2</sub>WO<sub>6</sub> heterostructure for the photocatalytic degradation of levofloxacin. *Opt. Mater.* **2020**, *107*, 110126. [[CrossRef](#)]
28. Yue, L.; Wang, S.; Shan, G.; Wu, W.; Qiang, L.; Zhu, L. Novel MWNTs–Bi<sub>2</sub>WO<sub>6</sub> composites with enhanced simulated solar photoactivity toward adsorbed and free tetracycline in water. *Appl. Catal. B-Environ.* **2015**, *176–177*, 11–19. [[CrossRef](#)]
29. Yan, F.; Wang, Y.; Yi, C.; Xu, J.; Wang, B.; Ma, R.; Xu, M. Construction of carbon dots modified Cl-doped Bi<sub>2</sub>WO<sub>6</sub> hollow microspheres for boosting photocatalytic degradation of tetracycline under visible light irradiation. *Ceram. Int.* **2022**, *in press*. [[CrossRef](#)]
30. Liang, W.; Pan, J.; Duan, X.; Tang, H.; Xu, J.; Tang, G. Biomass carbon modified flower-like Bi<sub>2</sub>WO<sub>6</sub> hierarchical architecture with improved photocatalytic performance. *Ceram. Int.* **2020**, *46*, 3623–3630. [[CrossRef](#)]
31. Wang, T.; Liu, S.; Mao, W.; Bai, Y.; Chiang, K.; Shah, K.; Paz-Ferreiro, J. Novel Bi<sub>2</sub>WO<sub>6</sub> loaded N-biochar composites with enhanced photocatalytic degradation of rhodamine B and Cr(VI). *J. Hazard. Mater.* **2020**, *389*, 121827. [[CrossRef](#)] [[PubMed](#)]
32. Mao, W.; Zhang, L.; Liu, Y.; Wang, T.; Bai, Y.; Guan, Y. Facile assembled N, S-codoped corn straw biochar loaded Bi<sub>2</sub>WO<sub>6</sub> with the enhanced electron-rich feature for the efficient photocatalytic removal of ciprofloxacin and Cr(VI). *Chemosphere* **2021**, *263*, 127988. [[CrossRef](#)] [[PubMed](#)]
33. Kaur, M.; Mehta, S.K.; Devi, P.; Kansal, S.K. Bi<sub>2</sub>WO<sub>6</sub>/NH<sub>2</sub>-MIL-88B(Fe) heterostructure: An efficient sunlight driven photocatalyst for the degradation of antibiotic tetracycline in aqueous medium. *Adv. Powder Technol.* **2021**, *32*, 4788–4804. [[CrossRef](#)]
34. He, Y.; Wang, D.; Li, X.; Fu, Q.; Yin, L.; Yang, Q.; Chen, H. Photocatalytic degradation of tetracycline by metal-organic frameworks modified with Bi<sub>2</sub>WO<sub>6</sub> nanosheet under direct sunlight. *Chemosphere* **2021**, *284*, 131386. [[CrossRef](#)]
35. Li, Q.; Li, L.; Long, X.; Tu, Y.; Ling, L.; Gu, J.; Hou, L.; Xu, Y.; Liu, N.; Li, Z. Rational design of MIL-88A(Fe)/Bi<sub>2</sub>WO<sub>6</sub> heterojunctions as an efficient photocatalyst for organic pollutant degradation under visible light irradiation. *Opt. Mater.* **2021**, *118*, 111260. [[CrossRef](#)]
36. Tu, Y.; Ling, L.; Li, Q.; Long, X.; Liu, N.; Li, Z. Greatly enhanced photocatalytic activity over Bi<sub>2</sub>WO<sub>6</sub> by MIL-53(Fe) modification. *Opt. Mater.* **2020**, *110*, 110500. [[CrossRef](#)]
37. Zhang, X.; Yuan, N.; Chen, T.; Li, B.; Wang, Q. Fabrication of hydrangea-shaped Bi<sub>2</sub>WO<sub>6</sub>/ZIF-8 visible-light responsive photocatalysts for degradation of methylene blue. *Chemosphere* **2022**, *307*, 135949. [[CrossRef](#)]
38. Dai, X.; Feng, S.; Wu, W.; Zhou, Y.; Ye, Z.; Wang, Y.; Cao, X. Photocatalytic Degradation of Tetracycline by Z-Scheme Bi<sub>2</sub>WO<sub>6</sub>/ZIF-8. *J. Inorg. Organomet. Polym. Mater.* **2022**, *32*, 2371–2383. [[CrossRef](#)]
39. Qi, S.; Zhang, R.; Zhang, Y.; Liu, X.; Xu, H. Preparation and photocatalytic properties of Bi<sub>2</sub>WO<sub>6</sub>/g-C<sub>3</sub>N<sub>4</sub>. *Inorg. Chem. Commun.* **2021**, *132*, 108761. [[CrossRef](#)]
40. Zhao, Y.; Liang, X.; Wang, Y.; Shi, H.; Liu, E.; Fan, J.; Hu, X. Degradation and removal of Ceftriaxone sodium in aquatic environment with Bi<sub>2</sub>WO<sub>6</sub>/g-C<sub>3</sub>N<sub>4</sub> photocatalyst. *J. Colloid Interface Sci.* **2018**, *523*, 7–17. [[CrossRef](#)]
41. Chen, J.; Yang, Q.; Zhong, J.; Li, J.; Hu, C.; Deng, Z.; Duan, R. In-situ construction of direct Z-scheme Bi<sub>2</sub>WO<sub>6</sub>/g-C<sub>3</sub>N<sub>4</sub> composites with remarkably promoted solar-driven photocatalytic activity. *Mater. Chem. Phys.* **2018**, *217*, 207–215. [[CrossRef](#)]
42. Zhu, D.; Zhou, Q. Novel Bi<sub>2</sub>WO<sub>6</sub> modified by N-doped graphitic carbon nitride photocatalyst for efficient photocatalytic degradation of phenol under visible light. *Appl. Catal. B-Environ.* **2020**, *268*, 118426. [[CrossRef](#)]
43. Wang, Y.; Jiang, W.; Luo, W.; Chen, X.; Zhu, Y. Ultrathin nanosheets g-C<sub>3</sub>N<sub>4</sub>@Bi<sub>2</sub>WO<sub>6</sub> core-shell structure via low temperature reassembled strategy to promote photocatalytic activity. *Appl. Catal. B-Environ.* **2018**, *237*, 633–640. [[CrossRef](#)]
44. Zhang, M.; Zhang, Y.; Tang, L.; Zeng, G.; Wang, J.; Zhu, Y.; Feng, C.; Deng, Y.; He, W. Ultrathin Bi<sub>2</sub>WO<sub>6</sub> nanosheets loaded g-C<sub>3</sub>N<sub>4</sub> quantum dots: A direct Z-scheme photocatalyst with enhanced photocatalytic activity towards degradation of organic pollutants under wide spectrum light irradiation. *J. Colloid Interface Sci.* **2019**, *539*, 654–664. [[CrossRef](#)] [[PubMed](#)]
45. Gordanshekan, A.; Arabian, S.; Solaimany Nazar, A.R.; Farhadian, M.; Tangestaninejad, S. A comprehensive comparison of green Bi<sub>2</sub>WO<sub>6</sub>/g-C<sub>3</sub>N<sub>4</sub> and Bi<sub>2</sub>WO<sub>6</sub>/TiO<sub>2</sub> S-scheme heterojunctions for photocatalytic adsorption/ degradation of Cefixime: Artificial neural network, degradation pathway, and toxicity estimation. *Chem. Eng. J.* **2023**, *451*, 139067. [[CrossRef](#)]
46. Li, W.; Ding, X.; Wu, H.; Yang, H. In-situ hydrothermal synthesis of TiO<sub>2</sub>/Bi<sub>2</sub>WO<sub>6</sub> heterojunction with enhanced photocatalytic activity. *Mater. Lett.* **2018**, *227*, 272–275. [[CrossRef](#)]
47. Chen, G.; Wang, Y.; Shen, Q.; Xiong, X.; Ren, S.; Dai, G.; Wu, C. Fabrication of TiO<sub>2</sub> nanofibers assembled by Bi<sub>2</sub>WO<sub>6</sub> nanosheets with enhanced visible light photocatalytic activity. *Ceram. Int.* **2020**, *46*, 21304–21310. [[CrossRef](#)]
48. Lu, Q.; Dong, C.; Wei, F.; Li, J.; Wang, Z.; Mu, W.; Han, X. Rational fabrication of Bi<sub>2</sub>WO<sub>6</sub> decorated TiO<sub>2</sub> nanotube arrays for photocatalytic degradation of organic pollutants. *Mater. Res. Bull.* **2022**, *145*, 111563. [[CrossRef](#)]
49. Wang, Q.; Li, H.; Yu, X.; Jia, Y.; Chang, Y.; Gao, S. Morphology regulated Bi<sub>2</sub>WO<sub>6</sub> nanoparticles on TiO<sub>2</sub> nanotubes by solvothermal Sb<sup>3+</sup> doping as effective photocatalysts for wastewater treatment. *Electrochim. Acta* **2020**, *330*, 135167. [[CrossRef](#)]
50. Sun, M.; Yao, Y.; Ding, W.; Anandan, S. N/Ti<sup>3+</sup> co-doping biphasic TiO<sub>2</sub>/Bi<sub>2</sub>WO<sub>6</sub> heterojunctions: Hydrothermal fabrication and sonophotocatalytic degradation of organic pollutants. *J. Alloy. Compd.* **2020**, *820*, 153172. [[CrossRef](#)]
51. Liu, J.; Luo, Z.; Han, W.; Zhao, Y.; Li, P. Preparation of ZnO/Bi<sub>2</sub>WO<sub>6</sub> heterostructures with improved photocatalytic performance. *Mater. Sci. Semicon. Proc.* **2020**, *106*, 104761. [[CrossRef](#)]
52. Koutavarapu, R.; Babu, B.; Reddy, C.V.; Reddy, I.N.; Reddy, K.R.; Rao, M.C.; Aminabhavi, T.M.; Cho, M.; Kim, D.; Shim, J. ZnO nanosheets-decorated Bi<sub>2</sub>WO<sub>6</sub> nanolayers as efficient photocatalysts for the removal of toxic environmental pollutants and photoelectrochemical solar water oxidation. *J. Environ. Manag.* **2020**, *265*, 110504. [[CrossRef](#)] [[PubMed](#)]

53. Chen, X.; Li, J.; Chen, F. Photocatalytic degradation of MB by novel and environmental ZnO/Bi<sub>2</sub>WO<sub>6</sub>-CC hierarchical heterostructures. *Mater. Charact.* **2022**, *189*, 111961. [[CrossRef](#)]
54. Zhao, F.; Gao, D.; Zhu, X.; Dong, Y.; Liu, X.; Li, H. Rational design of multifunctional C/N-doped ZnO/Bi<sub>2</sub>WO<sub>6</sub> Z-scheme heterojunction for efficient photocatalytic degradation of antibiotics. *Appl. Surf. Sci.* **2022**, *587*, 152780. [[CrossRef](#)]
55. Salari, H.; Yaghmaei, H. Z-scheme 3D Bi<sub>2</sub>WO<sub>6</sub>/MnO<sub>2</sub> heterojunction for increased photoinduced charge separation and enhanced photocatalytic activity. *Appl. Surf. Sci.* **2020**, *532*, 147413. [[CrossRef](#)]
56. Mallikarjuna, K.; Kim, H. Bandgap-tuned ultra-small SnO<sub>2</sub>-nanoparticle-decorated 2D-Bi<sub>2</sub>WO<sub>6</sub> nanoplates for visible-light-driven photocatalytic applications. *Chemosphere* **2021**, *263*, 128185. [[CrossRef](#)]
57. Zhu, B.; Song, D.; Jia, T.; Sun, W.; Wang, D.; Wang, L.; Guo, J.; Jin, L.; Zhang, L.; Tao, H. Effective Visible Light-Driven Photocatalytic Degradation of Ciprofloxacin over Flower-like Fe<sub>3</sub>O<sub>4</sub>/Bi<sub>2</sub>WO<sub>6</sub> Composites. *ACS Omega* **2021**, *6*, 1647–1656. [[CrossRef](#)]
58. Zhang, X.; Zhang, H.; Yu, J.; Wu, Z.; Zhou, Q. Preparation of flower-like Co<sub>3</sub>O<sub>4</sub> QDs/Bi<sub>2</sub>WO<sub>6</sub> p-n heterojunction photocatalyst and its degradation mechanism of efficient visible-light-driven photocatalytic tetracycline antibiotics. *Appl. Surf. Sci.* **2022**, *585*, 152547. [[CrossRef](#)]
59. Koutavarapu, R.; Syed, K.; Pagidi, S.; Jeon, M.Y.; Rao, M.C.; Lee, D.Y.; Shim, J. An effective CuO/Bi<sub>2</sub>WO<sub>6</sub> heterostructured photocatalyst: Analyzing a charge-transfer mechanism for the enhanced visible-light-driven photocatalytic degradation of tetracycline and organic pollutants. *Chemosphere* **2022**, *287*, 132015. [[CrossRef](#)]
60. Chen, X.; Li, Y.; Li, L. Facet-engineered surface and interface design of WO<sub>3</sub>/Bi<sub>2</sub>WO<sub>6</sub> photocatalyst with direct Z-scheme heterojunction for efficient salicylic acid removal. *Appl. Surf. Sci.* **2020**, *508*, 144796. [[CrossRef](#)]
61. Liu, G.; Cui, P.; Liu, X.; Wang, X.; Liu, G.; Zhang, C.; Liu, M.; Chen, Y.; Xu, S. A facile preparation strategy for Bi<sub>2</sub>O<sub>4</sub>/Bi<sub>2</sub>WO<sub>6</sub> heterojunction with excellent visible light photocatalytic activity. *J. Solid State Chem.* **2020**, *290*, 121542. [[CrossRef](#)]
62. Chao, P.Y.; Chang, C.J.; Lin, K.S.; Wang, C.F. Synergistic effects of morphology control and calcination on the activity of flower-like Bi<sub>2</sub>WO<sub>6</sub>-Bi<sub>2</sub>O<sub>3</sub> photocatalysts prepared by an ionic liquid-assisted solvothermal method. *J. Alloy. Compd.* **2021**, *883*, 160920. [[CrossRef](#)]
63. Qin, Y.; Li, H.; Lu, J.; Ding, Y.; Ma, C.; Liu, X.; Meng, M.; Yan, Y. Fabrication of Bi<sub>2</sub>WO<sub>6</sub>/In<sub>2</sub>O<sub>3</sub> photocatalysts with efficient photocatalytic performance for the degradation of organic pollutants: Insight into the role of oxygen vacancy and heterojunction. *Adv. Powder Technol.* **2020**, *31*, 2890–2900. [[CrossRef](#)]
64. Tang, Q.Y.; Chen, W.F.; Lv, Y.R.; Yang, S.Y.; Xu, Y.H. Z-scheme hierarchical Cu<sub>2</sub>S/Bi<sub>2</sub>WO<sub>6</sub> composites for improved photocatalytic activity of glyphosate degradation under visible light irradiation. *Sep. Purif. Technol.* **2020**, *236*, 116243. [[CrossRef](#)]
65. Zhang, Y.; Ju, P.; Hao, L.; Zhai, X.; Jiang, F.; Sun, C. Novel Z-scheme MoS<sub>2</sub>/Bi<sub>2</sub>WO<sub>6</sub> heterojunction with highly enhanced photocatalytic activity under visible light irradiation. *J. Alloy. Compd.* **2021**, *854*, 157224. [[CrossRef](#)]
66. Xie, T.; Liu, Y.; Wang, H.; Wu, Z. Layered MoSe<sub>2</sub>/Bi<sub>2</sub>WO<sub>6</sub> composite with P-N heterojunctions as a promising visible-light induced photocatalyst. *Appl. Surf. Sci.* **2018**, *444*, 320–329. [[CrossRef](#)]
67. Kumar, G.; Dutta, R.K. Fabrication of plate-on-plate SnS<sub>2</sub>/Bi<sub>2</sub>WO<sub>6</sub> nanocomposite as photocatalyst for sunlight mediated degradation of antibiotics in aqueous medium. *J. Phys. Chem. Solids* **2022**, *164*, 110639. [[CrossRef](#)]
68. Su, M.; Sun, H.; Tian, Z.; Zhao, Z.; Li, P. Z-scheme 2D/2D WS<sub>2</sub>/Bi<sub>2</sub>WO<sub>6</sub> heterostructures with enhanced photocatalytic performance. *Appl. Catal. A-Gen.* **2022**, *631*, 118485. [[CrossRef](#)]
69. Su, Y.; Xu, X.; Li, R.; Luo, X.; Yao, H.; Fang, S.; Peter Homewood, K.; Huang, Z.; Gao, Y.; Chen, X. Design and fabrication of a CdS QDs/Bi<sub>2</sub>WO<sub>6</sub> monolayer S-scheme heterojunction configuration for highly efficient photocatalytic degradation of trace ethylene in air. *Chem. Eng. J.* **2022**, *429*, 132241. [[CrossRef](#)]
70. Zhang, Z.; Lin, Y.; Liu, F. Preparation and photocatalytic performance of CdS@Bi<sub>2</sub>WO<sub>6</sub> hybrid nanocrystals. *J. Alloy. Compd.* **2021**, *889*, 161668. [[CrossRef](#)]
71. Xu, F.; Xu, C.; Chen, H.; Wu, D.; Gao, Z.; Ma, X.; Zhang, Q.; Jiang, K. The synthesis of Bi<sub>2</sub>S<sub>3</sub>/2D-Bi<sub>2</sub>WO<sub>6</sub> composite materials with enhanced photocatalytic activities. *J. Alloy. Compd.* **2019**, *780*, 634–642. [[CrossRef](#)]
72. He, Z.; Siddique, M.S.; Yang, H.; Xia, Y.; Su, J.; Tang, B.; Wang, L.; Kang, L.; Huang, Z. Novel Z-scheme In<sub>2</sub>S<sub>3</sub>/Bi<sub>2</sub>WO<sub>6</sub> core-shell heterojunctions with synergistic enhanced photocatalytic degradation of tetracycline hydrochloride. *J. Clean. Prod.* **2022**, *339*, 130634. [[CrossRef](#)]
73. Lu, X.; Che, W.; Hu, X.; Wang, Y.; Zhang, A.; Deng, F.; Luo, S.; Dionysiou, D.D. The facile fabrication of novel visible-light-driven Z-scheme CuInS<sub>2</sub>/Bi<sub>2</sub>WO<sub>6</sub> heterojunction with intimate interface contact by in situ hydrothermal growth strategy for extraordinary photocatalytic performance. *Chem. Eng. J.* **2019**, *356*, 819–829. [[CrossRef](#)]
74. Shangguan, X.Y.; Fang, B.L.; Xu, C.X.; Tan, Y.; Chen, Y.G.; Xia, Z.J.; Chen, W. Fabrication of direct Z-scheme FeIn<sub>2</sub>S<sub>4</sub>/Bi<sub>2</sub>WO<sub>6</sub> hierarchical heterostructures with enhanced photocatalytic activity for tetracycline hydrochloride photodegradation. *Ceram. Int.* **2021**, *47*, 6318–6328. [[CrossRef](#)]
75. Guo, M.; Zhou, Z.; Yan, S.; Zhou, P.; Miao, F.; Liang, S.; Wang, J.; Cui, X. Bi<sub>2</sub>WO<sub>6</sub>-BiOCl heterostructure with enhanced photocatalytic activity for efficient degradation of oxytetracycline. *Sci. Rep.* **2020**, *10*, 18401. [[CrossRef](#)]
76. Liang, Z.; Zhou, C.; Yang, J.; Mo, Q.; Zhang, Y.; Tang, Y. Visible light responsive Bi<sub>2</sub>WO<sub>6</sub>/BiOCl heterojunction with enhanced photocatalytic activity for degradation of tetracycline and rohdamine B. *Inorg. Chem. Commun.* **2018**, *93*, 136–139. [[CrossRef](#)]

77. Liu, K.; Zhang, H.; Muhammad, Y.; Fu, T.; Tang, R.; Tong, Z.; Wang, Y. Fabrication of n-n isotype BiOBr- Bi<sub>2</sub>WO<sub>6</sub> heterojunctions by inserting Bi<sub>2</sub>WO<sub>6</sub> nanosheets onto BiOBr microsphere for the superior photocatalytic degradation of Ciprofloxacin and tetracycline. *Sep. Purif. Technol.* **2021**, *274*, 118992. [[CrossRef](#)]
78. Ren, X.; Wu, K.; Qin, Z.; Zhao, X.; Yang, H. The construction of type II heterojunction of Bi<sub>2</sub>WO<sub>6</sub>/BiOBr photocatalyst with improved photocatalytic performance. *J. Alloy. Compd.* **2019**, *788*, 102–109. [[CrossRef](#)]
79. Chen, X.; Zhao, B.; Ma, J.; Liu, L.; Luo, H.; Wang, W. The BiOBr/Bi<sub>2</sub>WO<sub>6</sub> photocatalyst with SPR effect and Z-scheme heterojunction synergistically degraded RhB under visible light. *Opt. Mater.* **2021**, *122*, 111641. [[CrossRef](#)]
80. He, J.; Liu, Y.; Wang, M.; Wang, Y.; Long, F. Ionic liquid-hydrothermal synthesis of Z-scheme BiOBr/Bi<sub>2</sub>WO<sub>6</sub> heterojunction with enhanced photocatalytic activity. *J. Alloy. Compd.* **2021**, *865*, 158760. [[CrossRef](#)]
81. Huang, X.; Guo, Q.; Yan, B.; Liu, H.; Chen, K.; Wei, S.; Wu, Y.; Wang, L. Study on photocatalytic degradation of phenol by BiOI/Bi<sub>2</sub>WO<sub>6</sub> layered heterojunction synthesized by hydrothermal method. *J. Mol. Liq.* **2021**, *322*, 114965. [[CrossRef](#)]
82. Zheng, X.; Chu, Y.; Miao, B.; Fan, J. Ag-doped Bi<sub>2</sub>WO<sub>6</sub>/BiOI heterojunction used as photocatalyst for the enhanced degradation of tetracycline under visible-light and biodegradability improvement. *J. Alloy. Compd.* **2022**, *893*, 162382. [[CrossRef](#)]
83. Qiang, Z.; Liu, X.; Li, F.; Li, T.; Zhang, M.; Singh, H.; Huttula, M.; Cao, W. Iodine doped Z-scheme Bi<sub>2</sub>O<sub>2</sub>CO<sub>3</sub>/ Bi<sub>2</sub>WO<sub>6</sub> photocatalysts: Facile synthesis, efficient visible light photocatalysis, and photocatalytic mechanism. *Chem. Eng. J.* **2021**, *403*, 126327. [[CrossRef](#)]
84. Wu, R.; Song, H.; Luo, N.; Ji, G. Hydrothermal preparation of 3D flower-like BiPO<sub>4</sub>/Bi<sub>2</sub>WO<sub>6</sub> microsphere with enhanced visible-light photocatalytic activity. *J. Colloid Interface Sci.* **2018**, *524*, 350–359. [[CrossRef](#)] [[PubMed](#)]
85. Zhang, Y.; Xu, C.; Wan, F.; Zhou, D.; Yang, L.; Gu, H.; Xiong, J. Synthesis of flower-like Bi<sub>2</sub>Sn<sub>2</sub>O<sub>7</sub>/Bi<sub>2</sub>WO<sub>6</sub> hierarchical composites with enhanced visible light photocatalytic performance. *J. Alloy. Compd.* **2019**, *788*, 1154–1161. [[CrossRef](#)]
86. Tao, R.; Li, X.; Li, X.; Liu, S.; Shao, C.; Liu, Y. Discrete heterojunction nanofibers of BiFeO<sub>3</sub>/Bi<sub>2</sub>WO<sub>6</sub>: Novel architecture for effective charge separation and enhanced photocatalytic performance. *J. Colloid Interface Sci.* **2020**, *572*, 257–268. [[CrossRef](#)]
87. Teng, P.; Li, Z.; Gao, S.; Li, K.; Bowkett, M.; Copner, N.; Liu, Z.; Yang, X. Fabrication of one-dimensional Bi<sub>2</sub>WO<sub>6</sub>/CuBi<sub>2</sub>O<sub>4</sub> heterojunction nanofiber and its photocatalytic degradation property. *Opt. Mater.* **2021**, *121*, 111508. [[CrossRef](#)]
88. Wang, L.; Yang, G.; Wang, D.; Lu, C.; Guan, W.; Li, Y.; Deng, J.; Crittenden, J. Fabrication of the flower-flake-like CuBi<sub>2</sub>O<sub>4</sub>/Bi<sub>2</sub>WO<sub>6</sub> heterostructure as efficient visible-light driven photocatalysts: Performance, kinetics and mechanism insight. *Appl. Surf. Sci.* **2019**, *495*, 143521. [[CrossRef](#)]
89. Kumar, P.; Verma, S.; Korošin, N.Č.; Žener, B.; Štangar, U.L. Increasing the photocatalytic efficiency of ZnWO<sub>4</sub> by synthesizing a Bi<sub>2</sub>WO<sub>6</sub>/ZnWO<sub>4</sub> composite photocatalyst. *Catal. Today* **2022**, *397–399*, 278–285. [[CrossRef](#)]
90. Miao, B.; Chu, Y.; Zheng, X.; Su, H. Sb<sub>2</sub>WO<sub>6</sub>/Bi<sub>2</sub>WO<sub>6</sub> composite photocatalyst prepared by one-step hydrothermal method: Simple synthesis and excellent visible-light photocatalytic performance. *Mater. Sci. Semicon. Proc.* **2021**, *125*, 105636. [[CrossRef](#)]
91. Ni, Z.; Shen, Y.; Xu, L.; Xiang, G.; Chen, M.; Shen, N.; Li, K.; Ni, K. Facile construction of 3D hierarchical flower-like Ag<sub>2</sub>WO<sub>4</sub>/Bi<sub>2</sub>WO<sub>6</sub> Z-scheme heterojunction photocatalyst with enhanced visible light photocatalytic activity. *Appl. Surf. Sci.* **2022**, *576*, 151868. [[CrossRef](#)]
92. Zhang, R.; Zeng, K. A novel flower-like dual Z-scheme BiSI/Bi<sub>2</sub>WO<sub>6</sub>/g-C<sub>3</sub>N<sub>4</sub> photocatalyst has excellent photocatalytic activity for the degradation of organic pollutants under visible light. *Diam. Relat. Mater.* **2021**, *115*, 108343. [[CrossRef](#)]
93. Sun, H.; Zou, C.; Tang, W. Designing double Z-scheme heterojunction of g-C<sub>3</sub>N<sub>4</sub>/Bi<sub>2</sub>MoO<sub>6</sub>/Bi<sub>2</sub>WO<sub>6</sub> for efficient visible-light photocatalysis of organic pollutants. *Colloids Surf. A* **2022**, *654*, 130105. [[CrossRef](#)]
94. Zhou, K.; Liu, Y.; Hao, J. One-pot hydrothermal synthesis of dual Z-scheme BiOBr/g-C<sub>3</sub>N<sub>4</sub>/Bi<sub>2</sub>WO<sub>6</sub> and photocatalytic degradation of tetracycline under visible light. *Mater. Lett.* **2020**, *281*, 128463. [[CrossRef](#)]
95. Chu, Y.; Fan, J.; Wang, R.; Liu, C.; Zheng, X. Preparation and immobilization of Bi<sub>2</sub>WO<sub>6</sub>/BiOI/g-C<sub>3</sub>N<sub>4</sub> nanoparticles for the photocatalytic degradation of tetracycline and municipal waste transfer station leachate. *Sep. Purif. Technol.* **2022**, *300*, 121867. [[CrossRef](#)]
96. Hu, H.; Kong, W.; Wang, J.; Liu, C.; Cai, Q.; Kong, Y.; Zhou, S.; Yang, Z. Engineering 2D compressed layered g-C<sub>3</sub>N<sub>4</sub> nanosheets by the intercalation of BiVO<sub>4</sub>-Bi<sub>2</sub>WO<sub>6</sub> composites for boosting photocatalytic activities. *Appl. Surf. Sci.* **2021**, *557*, 149796. [[CrossRef](#)]
97. Wu, K.; Song, S.; Wu, H.; Guo, J.; Zhang, L. Facile synthesis of Bi<sub>2</sub>WO<sub>6</sub>/C<sub>3</sub>N<sub>4</sub>/Ti<sub>3</sub>C<sub>2</sub> composite as Z-scheme photocatalyst for efficient ciprofloxacin degradation and H<sub>2</sub> production. *Appl. Catal. A-Gen.* **2020**, *608*, 117869. [[CrossRef](#)]
98. Li, Q.; Lu, M.; Wang, W.; Zhao, W.; Chen, G.; Shi, H. Fabrication of 2D/2D g-C<sub>3</sub>N<sub>4</sub>/Au/Bi<sub>2</sub>WO<sub>6</sub> Z-scheme photocatalyst with enhanced visible-light-driven photocatalytic activity. *Appl. Surf. Sci.* **2020**, *508*, 144182. [[CrossRef](#)]
99. Jia, J.; Zhang, X.; Jiang, C.; Huang, W.; Wang, Y. Visible-light-driven nitrogen-doped carbon quantum dots decorated g-C<sub>3</sub>N<sub>4</sub>/Bi<sub>2</sub>WO<sub>6</sub> Z-scheme composite with enhanced photocatalytic activity and mechanism insight. *J. Alloy. Compd.* **2020**, *835*, 155180. [[CrossRef](#)]
100. Guan, Z.; Li, X.; Wu, Y.; Chen, Z.; Huang, X.; Wang, D.; Yang, Q.; Liu, J.; Tian, S.; Chen, X.; et al. AgBr nanoparticles decorated 2D/2D GO/Bi<sub>2</sub>WO<sub>6</sub> photocatalyst with enhanced photocatalytic performance for the removal of tetracycline hydrochloride. *Chem. Eng. J.* **2021**, *410*, 128283. [[CrossRef](#)]
101. Mengting, Z.; Kurniawan, T.A.; Yanping, Y.; Avtar, R.; Othman, M.H.D. 2D Graphene oxide (GO) doped p-n type BiOI/Bi<sub>2</sub>WO<sub>6</sub> as a novel composite for photodegradation of bisphenol A (BPA) in aqueous solutions under UV-vis irradiation. *Mater. Sci. Eng. C-Mater.* **2020**, *108*, 110420. [[CrossRef](#)] [[PubMed](#)]

102. Tian, J.; Zhu, Z.; Liu, B. Novel Bi<sub>2</sub>MoO<sub>6</sub>/Bi<sub>2</sub>WO<sub>6</sub>/MWCNTs photocatalyst with enhanced photocatalytic activity towards degradation of RB-19 under visible light irradiation. *Colloid. Surf. A* **2019**, *581*, 123798. [[CrossRef](#)]
103. Niu, J.; Song, Z.; Gao, X.; Ji, Y.; Zhang, Y. Construction of Bi<sub>2</sub>WO<sub>6</sub> composites with carbon-coated Cu<sub>2</sub>O for effective degradation of tetracycline. *J. Alloy. Compd.* **2021**, *884*, 161292. [[CrossRef](#)]
104. Wang, X.; Liu, X.; Li, H.; Yang, Y.; Ren, Y. Ag<sub>2</sub>CO<sub>3</sub>/AgBr/Bi<sub>2</sub>WO<sub>6</sub> nanocomposite: Synthesis and solar photocatalytic activity. *Inorg. Chem. Commun.* **2021**, *132*, 108826. [[CrossRef](#)]
105. Gan, W.; Zhang, J.; Niu, H.; Bao, L.; Hao, H.; Yan, Y.; Wu, K.; Fu, X. Fabrication of Ag/AgBr/Bi<sub>2</sub>WO<sub>6</sub> hierarchical composites with high visible light photocatalytic activity. *Chem. Phys. Lett.* **2019**, *737*, 136830. [[CrossRef](#)]
106. Jin, K.; Qin, M.; Li, X.; Wang, R.; Zhao, Y.; Wang, H. Z-scheme Au@TiO<sub>2</sub>/Bi<sub>2</sub>WO<sub>6</sub> heterojunction as efficient visible-light photocatalyst for degradation of antibiotics. *J. Mol. Liq.* **2022**, *364*, 120017. [[CrossRef](#)]
107. Mengting, Z.; Kurniawan, T.A.; Yanping, Y.; Dzarfan Othman, M.H.; Avtar, R.; Fu, D.; Hwang, G.H. Fabrication, characterization, and application of ternary magnetic recyclable Bi<sub>2</sub>WO<sub>6</sub>/BiOI@Fe<sub>3</sub>O<sub>4</sub> composite for photodegradation of tetracycline in aqueous solutions. *J. Environ. Manag.* **2020**, *270*, 110839. [[CrossRef](#)]
108. Chen, Y.; Su, X.; Ma, M.; Hou, Y.; Lu, C.; Wan, F.; Ma, Y.; Xu, Z.; Liu, Q.; Hao, M.; et al. One-dimensional magnetic flower-like CoFe<sub>2</sub>O<sub>4</sub>@Bi<sub>2</sub>WO<sub>6</sub>@BiOBr composites for visible-light catalytic degradation of Rhodamine B. *J. Alloy. Compd.* **2022**, *929*, 167297. [[CrossRef](#)]
109. Rao, C.; Zhou, L.; Pan, Y.; Lu, C.; Qin, X.; Sakiyama, H.; Muddassir, M.; Liu, J. The extra-large calixarene-based MOFs-derived hierarchical composites for photocatalysis of dye: Facile syntheses and contribution of carbon species. *J. Alloy. Compd.* **2022**, *897*, 163178. [[CrossRef](#)]
110. Jin, J.C.; Wang, J.; Guo, J.; Yan, M.H.; Wang, J.; Srivastava, D.; Kumar, A.; Sakiyama, H.; Muddassir, M.; Pan, Y. A 3D rare cubane-like tetramer Cu(II)-based MOF with 4-fold dia topology as an efficient photocatalyst for dye degradation. *Colloid. Surf. A* **2023**, *656*, 130475. [[CrossRef](#)]
111. Li, L.; Zou, J.; Han, Y.; Liao, Z.; Lu, P.; Nezamzadeh-Ejhieh, A.; Liu, J.; Peng, Y. Recent advances in Al(iii)/In(iii)-based MOFs for the detection of pollutants. *New J. Chem.* **2022**, *46*, 19577–19592. [[CrossRef](#)]
112. Sharma, V.; Kumar, A.; Kumar, A.; Krishnan, V. Enhanced photocatalytic activity of two dimensional ternary nanocomposites of ZnO-Bi<sub>2</sub>WO<sub>6</sub>-Ti<sub>3</sub>C<sub>2</sub> MXene under natural sunlight irradiation. *Chemosphere* **2022**, *287*, 132119. [[CrossRef](#)] [[PubMed](#)]
113. Ma, Q.; Ming, J.; Sun, X.; Liu, N.; Chen, G.; Yang, Y. Visible light active graphene oxide modified Ag/Ag<sub>2</sub>O/ BiPO<sub>4</sub>/Bi<sub>2</sub>WO<sub>6</sub> for photocatalytic removal of organic pollutants and bacteria in wastewater. *Chemosphere* **2022**, *306*, 135512. [[CrossRef](#)] [[PubMed](#)]